JACS
JOURNAL OF THE AMERICAN CHEMICAL SOCIETY

Article

pubs.acs.org/JACS

Significant Improvement of Semiconducting Performance of the Diketopyrrolopyrrole−Quaterthiophene Conjugated Polymer through Side-Chain Engineering via Hydrogen-Bonding

Jingjing Yao, Chenmin Yu, Zitong Liu,* Hewei Luo, Yang Yang, Guanxin Zhang, and Deqing Zhang*,†

Beijing National Laboratory for Molecular Sciences, Organic Solids Laboratory, Institute of Chemistry, Chinese Academy of Sciences, Beijing 100190, China

Supporting Information

ABSTRACT: Three diketopyrrolopyrrole (DPP)−quaterthiophene conjugated polymers, **pDPP4T-1**, **pDPP4T-2**, and **pDPP4T-3**, in which the molar ratios of the urea-containing alkyl chains vs branching alkyl chains are 1:30, 1:20, and 1:10, respectively, were prepared and investigated. In comparison with **pDPP4T** without urea groups in the alkyl side chains and **pDPP4T-A**, **pDPP4T-B**, and **pDPP4T-C** containing both linear and branched alkyl chains, thin films of **pDPP4T-1**, **pDPP4T-2**, and **pDPP4T-3** exhibit higher hole mobilities; thin-film mobility increases in the order **pDPP4T-1** < **pDPP4T-2** < **pDPP4T-3**, and hole mobility of a thin film of **pDPP4T-3** can reach 13.1 $cm^2 V^{-1} s^{-1}$ after thermal annealing at just 100 °C. The incorporation of urea groups in the alkyl side chains also has an interesting effect on the photovoltaic performances of DPP−quaterthiophene conjugated polymers after blending with $PC_{71}BM$. Blended thin films of **pDPP4T-1**:$PC_{71}BM$, **pDPP4T-2**:$PC_{71}BM$, and **pDPP4T-3**:$PC_{71}BM$ exhibit higher power conversion efficiencies (PCEs) than **pDPP4T**:$PC_{71}BM$, **pDPP4T-A**:$PC_{71}BM$, **pDPP4T-B**:$PC_{71}BM$, and **pDPP4T-C**:$PC_{71}BM$. The PCE of **pDPP4T-1**:$PC_{71}BM$ reaches 6.8%. Thin films of **pDPP4T-1**, **pDPP4T-2**, and **pDPP4T-3** and corresponding thin films with $PC_{71}BM$ were characterized with AFM, GIXRD, and STEM. The results reveal that the lamellar packing order of the alkyl chains is obviously enhanced for thin films of **pDPP4T-1**, **pDPP4T-2**, and **pDPP4T-3**; after thermal annealing, slight inter-chain $\pi-\pi$ stacking emerges for **pDPP4T-2** and **pDPP4T-3**. Blends of **pDPP4T-1**, **pDPP4T-2**, and **pDPP4T-3** with $PC_{71}BM$ show a more pronounced micro-phase separation. These observations suggest that the presence of urea groups may further facilitate the assemblies of these conjugated polymers into nanofibers and ordered aggregation of $PC_{71}BM$.

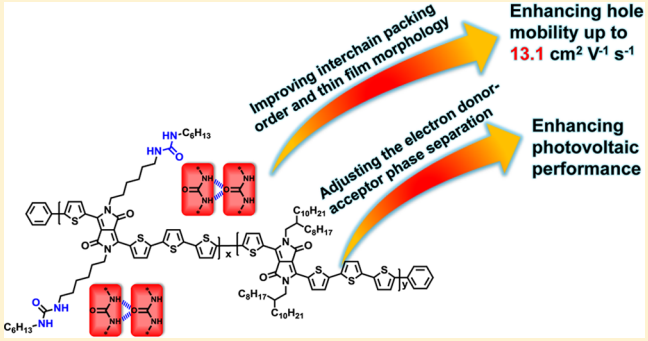

INTRODUCTION

As a new generation of semiconductors, conjugated polymers have received tremendous attention in the past decades because they show promising applications in low-cost, large-area, and flexible electronic devices, such as organic field-effect transistors (OFETs), organic solar cells (OSCs), and organic light-emitting diodes (OLEDs).[1−10] Among them conjugated electron donor (D) and acceptor (A) polymers have been extensively investigated.[11−26] These efforts have yielded *p*-type and *n*-type semiconductors with hole and electron mobilities up to 14.4 $cm^2 V^{-1} s^{-1}$[14] and 6.3 $cm^2 V^{-1} s^{-1}$,[16] respectively, by simple solution processing technique. Ambipolar semiconductors based on the conjugated D−A polymers have been also disclosed.[21,27] Moreover, a number of conjugated D−A polymers have been successfully utilized as either electron donors[24,25] or acceptors[26] for organic photovoltaic cells (OPVs) with power conversion efficiencies (PCEs) over 10%.[24]

Fundamental studies have been carried out to understand the influence of structure from the atomic and mesoscopic to macroscopic scales on the semiconducting performance for conjugated D−A polymers.[28,29] These studies manifest that apart from the conjugated backbones the alkyl side chains can dictate the self-organization of the polymer owing to the need for the side chains to form low-energy, space-filling structures. In many cases, the attractive van der Waals interactions between the alkyl side chains can exert an important influence on the inter-chain packing and backbone conformation, and as a result the thin-film microstructure and charge transporting are affected. For instance, Pei and co-workers reported the enhancement of charge mobility for isoindigo-based conjugated polymer after varying the branching alkyl chains by separating the branching point away from the conjugated backbone.[30] By employing similar strategy, both hole and electron mobilities increased for a selenophene-based diketopyrrolopyrrole (DPP) copolymer as reported by Yang, Oh, and their co-workers.[12] High charge mobility up to 12.04 $cm^2 V^{-1} s^{-1}$ was obtained for the DPP-based copolymers with alkyl side chains in which a

Received: September 16, 2015
Published: December 15, 2015

DOI: 10.1021/jacs.5b09737
J. Am. Chem. Soc. 2016, 138, 173−185

C6-spacer was inserted between the branching point and the backbone.[13] Fréchet and co-workers discovered that the DPP−thiophene copolymers with linear alkyl chains showed better photovoltaic performance than the respective conjugated polymers with branching chains.[31]

In this article we report the DPP−quaterthiophene conjugated polymers **pDPP4T-1**, **pDPP4T-2**, and **pDPP4T-3** (Scheme 1), in which part of the branching alkyl chains are replaced by urea-containing alkyl chains. The motivation of introducing urea groups in the side chains is illustrated in Scheme 1 and explained as follows: (i) It is known that urea groups can form hydrogen-bonding, and it is anticipated that such hydrogen-bonding will alter the inter-chain interactions, and consequently the semiconducting property can be tuned. (ii) The hydrogen-bonding due to urea groups may induce the polymer to form ordered and large domains, which is beneficial for charge transporting. Alternatively, such hydrogen-bonding may promote the inter-connection between polymer domains and accordingly facilitate the charge migration between domains. (iii) The formation of hydrogen-bonding among urea groups in the side chains may induce the self-aggregation of the polymers and thus tailor the donor−acceptor phase separation scales in blended thin films with appropriate electron acceptors. Therefore, the incorporation of urea groups in the side chains may usher in improving the photovoltaic performance. We demonstrate here that the side chain engineering via hydrogen-bonding is an effective strategy to enhance the semiconducting performance of conjugated D−A polymers. The thin-film hole mobility of **pDPP4T-3** in which the molar ratio between the urea-containing alkyl chains and branching alkyl chains is 1:10 increases from 3.4 $cm^2\ V^{-1}\ s^{-1}$ (for **pDPP4T** without urea groups) to 13.1 $cm^2\ V^{-1}\ s^{-1}$. Furthermore, **pDPP4T-1** with a molar ratio of 1:30 between the urea-containing alkyl chains and branching alkyl chains shows better photovoltaic performance after blending with $PC_{71}BM$ than **pDPP4T**.

Scheme 1. Chemical Structures of pDPP4T-1, pDPP4T-2, pDPP4T-3, and pDPP4T, and Illustration of the Design Rationale for Incorporation of Urea Groups in the Side Chains of Conjugated D−A Polymers

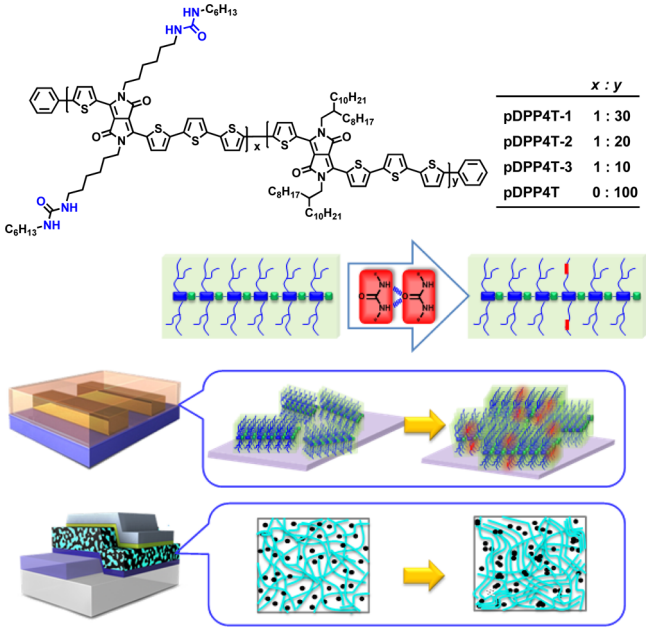

RESULTS AND DISCUSSION

Synthesis and Characterization. The synthesis of the conjugated polymers **pDPP4T-1**, **pDPP4T-2**, and **pDPP4T-3** entailing different amounts of urea groups in the side chains is outlined in Scheme 2. The co-polymerization of compounds **1**, **2**, and **3** under Stille coupling reaction condition yielded these conjugated polymers. Compounds **2**, **3**, and **4** are commercially available and used without any further purification. The synthesis of **1** started from compound **4** which was transformed into **5** in 45% yield after reaction with NaN_3. The reaction of **5** with triphenylphosphine yielded **6** in 68% yield. Then,

Scheme 2. Synthetic Approaches for pDPP4T-1, pDPP4T-2, and pDPP4T-3

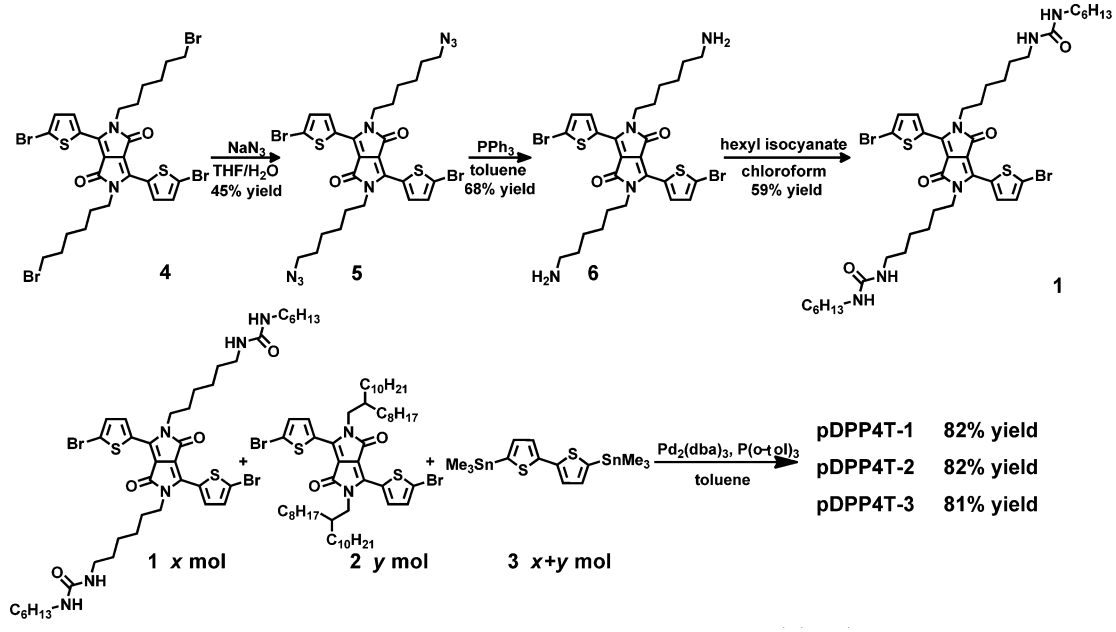

DOI: 10.1021/jacs.5b09737
J. Am. Chem. Soc. 2016, 138, 173−185

compound **6** was allowed to react with hexyl isocyanate to generate **1** in 59% yield after purification.

By varying the molar ratio between **1** and **2** from 1:30 to 1:20 and 1:10, conjugated polymers **pDPP4T-1**, **pDPP4T-2**, and **pDPP4T-3** were obtained. For comparison, **pDPP4T** without urea groups in the alkyl side chains was also prepared according to the reported procedure.[32a] Briefly, after the polymerization reaction, methanol was added to the reaction mixture to induce the precipitation of each polymer. Each precipitated polymer was subjected to Soxhlet extraction with methanol, hexane, and acetone to remove the remaining monomers and oligomers. After extracting with chloroform and precipitation in methanol again, **pDPP4T-1**, **pDPP4T-2**, **pDPP4T-3**, and **pDPP4T** were obtained in moderate yields. The chemical structures of **pDPP4T-1**, **pDPP4T-2**, and **pDPP4T-3** as well as **pDPP4T** were verified by ^{1}H NMR, solid-state ^{13}C NMR, and elemental analysis (see Experimental Section and Supporting Information). The elemental analysis results confirmed the molar ratios between the urea-containing alkyl chains and branching alkyl chains to be 1:30, 1:20, and 1:10 for **pDPP4T-1**, **pDPP4T-2**, and **pDPP4T-3**, respectively. Like **pDPP4T**, **pDPP4T-1**, **pDPP4T-2**, and **pDPP4T-3** can be dissolved in $CHCl_3$, 1,1,2,2-tetrachloroethane, toluene, and other aromatic solvents. The molecular weights (M_n) of **pDPP4T-1**, **pDPP4T-2**, **pDPP4T-3**, and **pDPP4T** were measured with gel permeation chromatography to be 28.4, 19.8, 16.6, and 18.8 kg mol^{-1}, with PDI of 2.66, 2.33, 2.54, and 2.14, respectively. On the basis of thermogravimetric analysis data shown in Figure S1a,b, the thermal decomposition temperatures (measured at 5% weight loss) of **pDPP4T-1**, **pDPP4T-2**, and **pDPP4T-3** as well as **pDPP4T** are all higher than 350 °C. Differential scanning calorimetry analyses were performed for all polymers, and no obvious thermal transitions were detected (see Figure S1c,d).

Typical stretching IR absorption around 3400 cm^{-1} due to urea groups was detected for **pDPP4T-1**, **pDPP4T-2**, and **pDPP4T-3**, whereas **pDPP4T** exhibited no IR absorption in this region (Figure 1). In order to further demonstrate the formation of inter-chain hydrogen-bonding, ^{1}H NMR spectra of **pDPP4T-2** were measured at different temperatures. Figure 1 shows the ^{1}H NMR spectra of **pDPP4T-2** in 1,1,2,2-tetrachloroethane-d_2 (1.0 mg/mL) at different temperatures. The ^{1}H NMR signal due to the urea group was detected at 5.43 ppm at 293 K. This agrees with the observation that the ^{1}H NMR signal of the urea group in **1** appears at 5.14 ppm at 373 K. This ^{1}H NMR signal was gradually upfield-shifted to 5.28 ppm at 333 K, 5.20 ppm at 353 K, and 5.15 ppm at 373 K. Moreover, this broad signal disappeared after further addition of D_2O. Such ^{1}H NMR signal shifts indicates the formation of inter-chain hydrogen-bonding due to urea groups in the side chains.

Electrochemical and Optical Properties. HOMO and LUMO levels of **pDPP4T-1**, **pDPP4T-2**, and **pDPP4T-3** were estimated from the respective onset oxidation and reduction potentials on the basis of their thin-film cyclic voltammograms as shown in Figure S2. For comparison, HOMO and LUMO energies of **pDPP4T** were also measured in the same way. As listed in Table 1, the HOMO and LUMO energies of **pDPP4T-1**, **pDPP4T-2**, and **pDPP4T-3** are around −5.29 and −3.58 eV, respectively. Consequently, the bandgaps of **pDPP4T-1**, **pDPP4T-2**, and **pDPP4T-3** are about 1.7 eV. In comparison with those of **pDPP4T**, HOMO levels of **pDPP4T-1**, **pDPP4T-2**, and **pDPP4T-3** are slightly enhanced, whereas LUMO levels are weakly lowered.

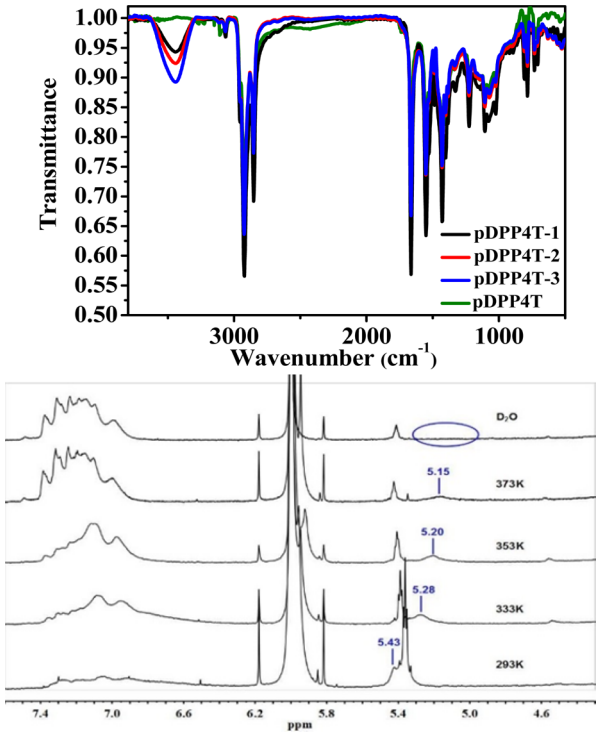

Figure 1. (Top) FT-IR spectra of **pDPP4T-1**, **pDPP4T-2**, **pDPP4T-3**, and **pDPP4T**. (Bottom) Variable-temperature ^{1}H NMR spectra (500 MHz) for **pDPP4T-2** in 1,1,2,2-tetrachloroethane-d_2 and that after addition of D_2O.

The absorption spectra of the solutions and thin films of **pDPP4T-1**, **pDPP4T-2**, **pDPP4T-3**, and **pDPP4T** were measured and shown in Figure 2. It is obvious that **pDPP4T-1**, **pDPP4T-2**, **pDPP4T-3**, and **pDPP4T** in solutions exhibit rather similar absorption spectra. In comparison with the respective absorption spectra of their solutions, the absorption around 725 nm emerges, and the absorption tail around 925 nm is enhanced for thin films of these polymers (see Figure 2B). The absorption spectra of thin films of these polymers are slightly different in terms of the absorptions around 725 and 925 nm. According to previous reports,[30,32b−d] such slight absorption spectral differences for thin films of **pDPP4T-1**, **pDPP4T-2**, and **pDPP4T-3** can be attributed to the inter-chain interactions which may entail hydrogen-bonding among urea groups in the side chains. On the basis of the respective onset absorptions of their thin films, the optical gaps of **pDPP4T-1**, **pDPP4T-2**, and **pDPP4T-3** were estimated to be around 1.34 eV (see Table 1).

Enhancement of Charge Carrier Mobility. To probe how hydrogen-bonding due to the urea groups in the side chains influences the charge transporting property for thin neat films of **pDPP4T-1**, **pDPP4T-2**, and **pDPP4T-3**, bottom-gate/bottom-contact (BGBC) field-effect transistors (FETs) were fabricated following conventional procedures (for details, see Supporting Information); these were measured in air. Figure 3 shows the respective transfer and output characteristics of FETs with thin films of these conjugated polymers after thermal annealing at 100 °C. They all exhibit typical *p*-type semiconducting behavior. The hole mobilities (μ_h) were extracted by fitting the linear part of the plot of $|I_{DS}|^{1/2}$ vs V_{GS}.[27,33−35]

DOI: 10.1021/jacs.5b09737
J. Am. Chem. Soc. 2016, 138, 173−185

Table 1. Absorption, Onset Redox Potentials, HOMO/LUMO Energies, and Band Gaps of pDPP4T-1, pDPP4T-2, pDPP4T-3, and pDPP4T

	λ_{max}[a] (nm) (ε_{max}, M^{-1} cm^{-1})[b]							
polymer	solution	film	E_{redl}^{onset} (V)[c]	E_{LUMO} (eV)[d]	E_{oxl}^{onset} (V)[c]	E_{HOMO} (eV)[d]	E_g^{cv} (eV)[e]	E_g^{opt} (eV)[f]
pDPP4T-1	784 (85 000)	726, 794	−1.25	−3.55	0.51	−5.31	1.76	1.34
pDPP4T-2	786 (84 000)	726, 792	−1.22	−3.58	0.49	−5.29	1.71	1.34
pDPP4T-3	782 (82 000)	722, 796	−1.20	−3.60	0.44	−5.24	1.64	1.32
pDPP4T	780 (84 000)	726, 794	−1.26	−3.54	0.52	−5.32	1.78	1.36

[a]Absorption maxima in $CHCl_3$ solution (1.0×10^{-5} M for each polymer) and the spin-coated thin film. [b]Molar extinction coefficient (ε_{max}, M^{-1} cm^{-1}). [c]Onset potentials (V vs Fc/Fc^+) for reduction (E_{redl}^{onset}) and oxidation (E_{oxl}^{onset}). [d]Estimated with the following equation: $E_{HOMO} = -(E_{oxl}^{onset} + 4.8)$ eV, $E_{LUMO} = -(E_{redl}^{onset} + 4.8)$ eV. [e]Based on redox potentials. [f]Based on the absorption spectral data.

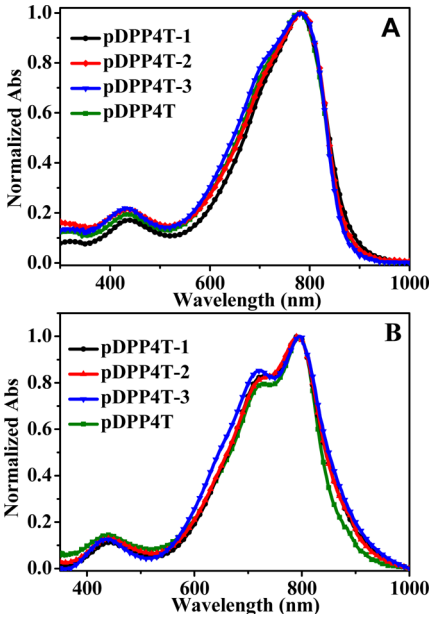

Figure 2. Normalized UV−vis absorption spectra of (A) **pDPP4T-1**, **pDPP4T-2**, **pDPP4T-3**, and **pDPP4T** in $CHCl_3$ (1.0×10^{-5} M) and (B) their thin films.

Apart from hole mobilities, threshold voltages (V_{Th}), I_{on}/I_{off} ratios, and sub-threshold slopes (SS), which reflect the semiconducting performances of **pDPP4T-1**, **pDPP4T-2**, and **pDPP4T-3**, are also included in Table 2. The hole mobility increased after thermal annealing at 100 °C for each of these conjugated polymers, but it decreased after further annealing at 120 °C. For instance, μ_h increased from 1.4 cm^2 V^{-1} s^{-1} for the as-prepared FET of **pDPP4T-1** to 5.5 cm^2 V^{-1} s^{-1} after thermal annealing at 100 °C, while it was reduced to 3.8 cm^2 V^{-1} s^{-1} after further thermal annealing at 120 °C. It is interesting to note that hole mobilities were incremented gradually by increasing the content of urea groups in the side chains; the average μ_h of the as-prepared FETs increased from 1.1 cm^2 V^{-1} s^{-1} for **pDPP4T-1** to 1.6 cm^2 V^{-1} s^{-1} for **pDPP4T-2** and to 5.7 cm^2 V^{-1} s^{-1} for **pDPP4T-3**, and average hole mobilities of FETs after thermal annealing at 100 °C were estimated to be 5.1, 7.1, and 11.4 cm^2 V^{-1} s^{-1} for **pDPP4T-1**, **pDPP4T-2**, and **pDPP4T-3**, respectively. Remarkably, hole mobility of the thin film of **pDPP4T-3** could reach 13.1 cm^2 V^{-1} s^{-1} after thermal annealing at 100 °C for 1.0 h. To the best of our knowledge, this is among the highest charge carrier moblities reported for conjugated polymers to date.[11−14,35a,b] Usually, thermal annealing at above 200 °C and even exceeding 300 °C is required to enable the conjugated polymers to exhibit high charge mobilities.[12,14,35c] For **pDPP4T-1**, **pDPP4T-2**, and

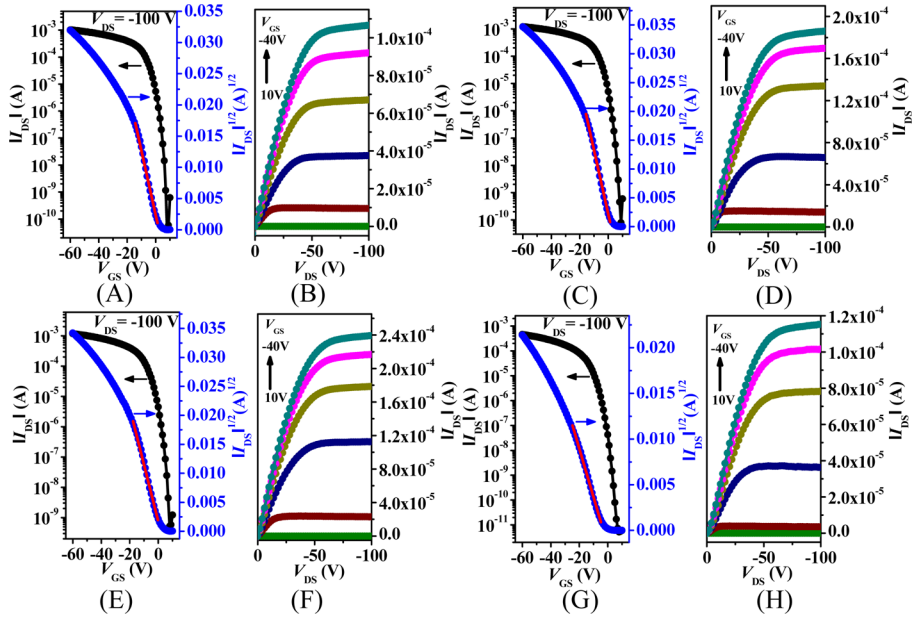

Figure 3. Transfer and output characteristics of BGBC FETs prepared with thin films of (A,B) **pDPP4T-1**, (C,D) **pDPP4T-2**, (E,F) **pDPP4T-3**, and (G,H) **pDPP4T** after annealing at the 100 °C. The channel width (W) and length (L) were 1440 and 50 μm, respectively.

DOI: 10.1021/jacs.5b09737
J. Am. Chem. Soc. 2016, 138, 173−185

Table 2. Hole Mobilities (Evaluated in the Saturated Regime, μ_h, and Linear Regime, μ_{lin}), Threshold Voltages (V_{Th}), I_{on}/I_{off} Ratios, and Subthreshold Slopes (SS) for BGBC FETs with pDPP4T-1, pDPP4T-2, pDPP4T-3, pDPP4T, pDPP4T-A, pDPP4T-B, and pDPP4T-C at Different Annealing Temperatures

polymer	temp (°C)	μ_h[a] ($cm^2\ V^{-1}\ s^{-1}$)	V_{Th} (V)	I_{on}/I_{off}	μ_{lin}[b] ($cm^2\ V^{-1}\ s^{-1}$)	SS[b] (V decade^{-1})
pDPP4T-1	RT	1.4/1.1	3−15	10^7−10^8		
	100	5.5/5.1	0−18	10^6−10^7	1.8/1.4	1.3−1.4
	120	3.8/3.5	−1 to 8	10^6−10^7		
pDPP4T-2	RT	1.8/1.6	20−36	10^7−10^8		
	100	8.4/7.1	1−14	10^6−10^7	2.8/2.1	1.8−2.0
	120	4.4/3.6	−7 to 5	10^6- 10^7		
pDPP4T-3	RT	6.3/5.7	3−7	10^6−10^7		
	100	13.1/11.4	2−18	10^6−10^7	3.3/2.6	1.6−2.0
	120	8.7/7.8	−3 to 10	10^6−10^7		
pDPP4T-A	RT	2.4/2.0	−1 to 9	10^6−10^7		
	100	4.4/3.6	−1 to 8	10^6−10^7	1.5/1.1	0.9−1.7
	120	3.8/3.4	0−10	10^6−10^7		
pDPP4T-B	RT	2.6/2.4	−2 to 6	10^6−10^7		
	100	5.1/4.8	−1 to 9	10^6−10^7	1.7/1.2	0.9−1.6
	120	4.7/4.1	−4 to 7	10^6−10^7		
pDPP4T-C	RT	2.6/2.4	−4 to 8	10^5−10^6		
	100	3.4/2.9	−2 to 7	10^5−10^6	0.9/0.7	1.8−2.1
	120	2.9/2.5	−5 to 8	10^5−10^6		
pDPP4T	RT	0.6/0.4	23−32	10^7−10^8		
	100	3.4/3.0	2−11	10^6−10^8	1.0/0.6	1.4−1.7
	120	1.4/1.3	−5 to 3	10^6−10^7		
reference[34d]	200	5.50/3.57	−7	10^6		

[a]The mobilities are provided in "highest/average" form, and the performance data are based on more than 15 different FETs. [b]The performance data were obtained after annealing of the thin films at 100 °C.

pDPP4T-3, in strong contrast, thermal annealing at much lower temperature can lead to high charge mobilities, which should drastically facilitate device fabrication (e.g., on flexible substrates that thermally often are less stable) and limits unwanted device degradation due to exposure to high temperatures.

For comparison, FETs comprising **pDPP4T** thin films were characterized at the same conditions. The hole mobility of an as-prepared FET with a thin film of **pDPP4T** was measured to be 0.6 $cm^2\ V^{-1}\ s^{-1}$, and it increased to 3.4 $cm^2\ V^{-1}\ s^{-1}$ after annealing under vacuum at 100 °C for 1.0 h.[36] Clearly, the mobilities of **pDPP4T-1**, **pDPP4T-2**, and **pDPP4T-3** are higher than those of **pDPP4T** both as-cast and after thermal annealing, while also displaying relatively high I_{on}/I_{off} ratios (10^6−10^8). It is clear that the incorporation of urea groups in the side chains of conjugated polymers can improve their charge transport behavior. Furthermore, higher charge mobilities are resulted when more urea groups are incorporated in the side chains of conjugated polymers. To further support this conclusion, the conjugated polymers, **pDPP4T-A**, **pDPP4T-B**, and **pDPP4T-C** (Scheme 3), in which the molar ratios of the linear chain vs the branched alkyl chain is 1:30, 1:20, and 1:10, respectively, were prepared and characterized (see Supporting Information). Their HOMO/LUMO energies and bandgaps were found to be similar to those of **pDPP4T** (see Table S1). The number-average molecular weight (M_n) values of **pDPP4T-A**, **pDPP4T-B**, and **pDPP4T-C** are 74.0 (PDI = 2.86), 91.5 (PDI = 2.09), and 94.6 kg mol^{-1} (PDI = 2.20), respectively. Bottom-gate/bottom-contact FETs with thin films of **pDPP4T-A**, **pDPP4T-B**, and **pDPP4T-C** were fabricated similarly. The respective transfer characteristics and output curves are displayed in Figure S4. Their hole mobilities were extracted in the same manner as for **pDPP4T-1**, **pDPP4T-2**, and **pDPP4T-3**, and the data are summarized in Table 2. Clearly, hole mobilities of thin films of **pDPP4T-1** and **pDPP4T-2** after thermal annealing at 100 °C are higher than those of **pDPP4T-A**, **pDPP4T-B**, respectively. Note that the

Scheme 3. Chemical Structures of pDPP4T-A, pDPP4T-B, and pDPP4T-C

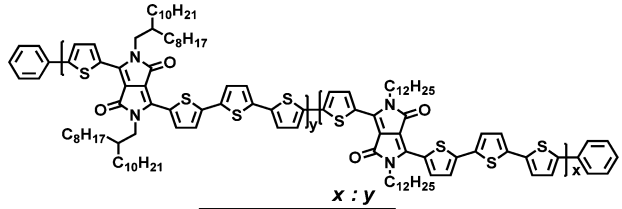

DOI: 10.1021/jacs.5b09737
J. Am. Chem. Soc. 2016, 138, 173−185

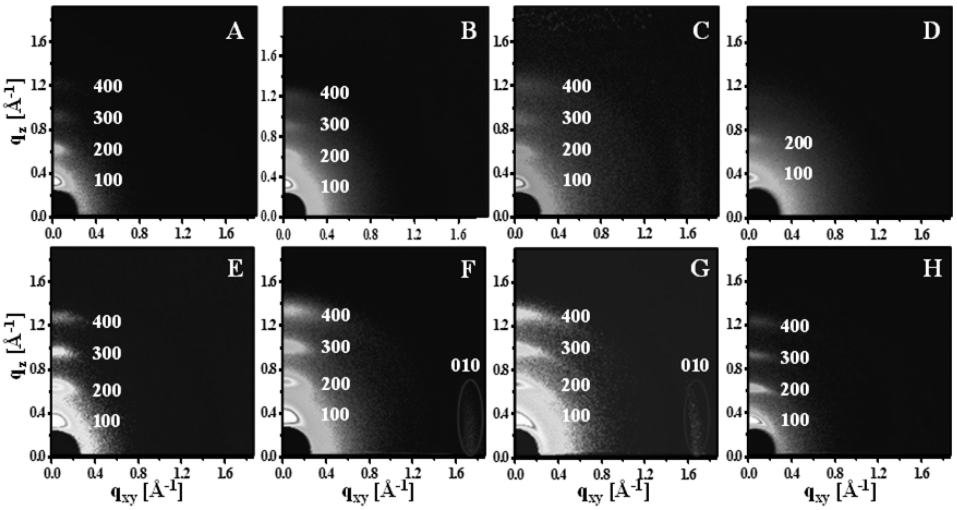

Figure 4. Grazing incidence X-ray diffraction patterns of (A,E) **pDPP4T-1**, (B,F) **pDPP4T-2**, (C,G) **pDPP4T-3**, and (D,H) **pDPP4T** deposited on OTS-modified SiO_2/Si substrates (top) at room temperature and (bottom) after thermal annealing at 100 °C.

as-prepared thin films of **pDPP4T-1** and **pDPP4T-2** do not exhibit higher hole mobilities than those of **pDPP4T-A** and **pDPP4T-B**, respectively. This may be understandable by considering the fact that molecular weights of **pDPP4T-A** and **pDPP4T-B** are obviously higher than those of **pDPP4T-1** and **pDPP4T-2** (see above). However, thin films of **pDPP4T-3** (both as-prepared and that after thermal annealing) show higher hole mobilities than those of **pDPP4T-C**; average hole mobilities of **pDPP4T-3** were estimated to be 5.7 and 11.4 cm^2 V^{-1} s^{-1} for the as-prepared thin film and that after thermal annealing at 100 °C, respectively, whereas those of **pDPP4T-C** were 2.4 and 2.9 cm^2 V^{-1} s^{-1} under the same conditions.

Hole mobilities evaluated in the linear regime were also extracted for thin films (after thermal annealing at 100 °C) of **pDPP4T-1**, **pDPP4T-2**, and **pDPP4T-3** as well those of **pDPP4T-A**, **pDPP4T-B**, and **pDPP4T-C** (see Table 2) according to previous procedures.[37] Again, hole mobilities in the linear region for thin films of **pDPP4T-1**, **pDPP4T-2**, and **pDPP4T-3** are higher than those of **pDPP4T-A**, **pDPP4T-B**, and **pDPP4T-C**, respectively. All these results clearly reveal that urea groups in the side chains of **pDPP4T-1**, **pDPP4T-2**, and **pDPP4T-3** are important for improving their charge mobilities.

Apart from BGBC FETs the bottom-gate/top-contact (BGTC) devices were also fabricated with thin films of **pDPP4T-1**, **pDPP4T-2**, and **pDPP4T-3** as well as those of **pDPP4T-A**, **pDPP4T-B**, and **pDPP4T-C**. Figure S5 shows the respective transfer and output curves of OFETs with thin films of these conjugated polymers after thermal annealing at 100 °C. As listed in Table S2, thin-film hole mobilities of **pDPP4T-1**, **pDPP4T-2**, and **pDPP4T-3** deduced from the characteristics of BGTC devices are higher than those of **pDPP4T-A**, **pDPP4T-B**, and **pDPP4T-C**, respectively. For instance, the highest hole mobility of the BGTC device with a thin film of **pDPP4T-3** is 8.8 cm^2 V^{-1} s^{-1}, while that with a thin film of **pDPP4T-C** can just reach 2.6 cm^2 V^{-1} s^{-1}.[38,39]

In addition, the stability of BGBC FETs fabricated with **pDPP4T-1**, **pDPP4T-2**, and **pDPP4T-3** was assessed over a period of 30 days, in air with an average humidity of 30%. As depicted in Figure S6, hole mobilities of **pDPP4T-1**, **pDPP4T-2**, and **pDPP4T-3** slightly decreased for the first 2 days and then remained almost unchanged after the devices were left in ambient condition for 30 days. Similarly, the I_{on}/I_{off} ratios remained relatively high for these FETs even after being left in air for even 30 days.

GIXRD Characterization for Thin Films of These Conjugated Polymers. In order to elucidate the remarkable enhancement of charge mobility after incorporation of urea groups in the side chains as in **pDPP4T-1**, **pDPP4T-2**, and **pDPP4T-3**, thin films of these conjugated polymers were characterized with grazing-incidence X-ray diffractions (GIXRD) and atomic force microscopy (AFM). Figure 4 shows the 2D GIXRD patterns of thin films of these polymers before and after thermal annealing at 100 °C. Four diffractions along the q_z direction, corresponding to the (100), (200), (300), and (400) ones, were detected for the as-prepared thin films of **pDPP4T-1**, at q_z = 0.30, 0.62, 0.94, and 1.25 Å^{-1}. The corresponding *d*-spacing was determined to be 20.29 Å. Similarly, four diffraction signals at q_z = 0.31, 0.62, 0.93, and 1.25 Å^{-1} were detected for the as-prepared thin film of **pDPP4T-2**, corresponding to a *d*-spacing of 20.25 Å. The as-prepared thin film of **pDPP4T-3** also displayed four diffractions at q_z = 0.31, 0.63, 0.94, and 1.26 Å^{-1}, corresponding to a *d*-spacing of 20.07 Å. No diffractions along the q_{xy} direction were detected for all the as-prepared thin films. We conclude from these GIXRD data that the alkyl chains in **pDPP4T-1**, **pDPP4T-2**, and **pDPP4T-3** adopt well-defined lamellar packing up to the fourth order. In comparison, only the first-order (at q_z = 0.31 Å^{-1}) and weak second-order (at q_z = 0.62 Å^{-1}) diffractions along the q_z direction were observed for thin films of **pDPP4T**. Obviously, the degree of order for the lamellar stacking of the alkyl chains increases after incorporation of urea groups in the alkyl side chains of **pDPP4T-1**, **pDPP4T-2**, and **pDPP4T-3**.

After thermal annealing at 100 °C the intensities of diffraction signals along the q_z direction were obviously enhanced for thin films of **pDPP4T-1**, **pDPP4T-2**, and **pDPP4T-3**. Moreover, thermal annealing led to new diffractions along the q_{xy} direction at $q_{xy} \approx$ 1.68 and 1.67 Å^{-1} for **pDPP4T-2** and **pDPP4T-3**, respectively. The corresponding *d*-spacing is 3.74 and 3.75 Å for thin films of **pDPP4T-2** and **pDPP4T-3**, respectively. We therefore attribute these features to some weak $\pi-\pi$ interactions developing between the polymer conjugated backbones.[32a]

DOI: 10.1021/jacs.5b09737
J. Am. Chem. Soc. 2016, 138, 173−185

Alternatively, the 1D diffraction profiles for the *out-of-plane* direction were also collected for the as-prepared thin films of **pDPP4T-1**, **pDPP4T-2**, and **pDPP4T-3** and those after thermal annealing at 100 and 120 °C (see Figure S7).[40] As shown in Figure S7 four diffractions were detected for each conjugated polymer. For instance, the corresponding (100), (200), (300), and (400) diffractions, were detected for the as-prepared thin film of **pDPP4T-3**, at q_z = 0.31, 0.63, 0.95, and 1.24 Å^{-1}. For thin films of **pDPP4T-1**, **pDPP4T-2**, and **pDPP4T-3**, the intensities of *out-of-plane* diffractions, in particular the (100) and (200) ones, increased after thermal annealing at 100 °C. But, the diffraction intensities increased only slightly after further annealing at 120 °C. Moreover, the *out-of-plane* diffractions were compared for **pDPP4T-1**, **pDPP4T-2**, and **pDPP4T-3** after thermal annealing at 100 °C (see Figure S9); the diffraction intensities were incremented in the following order: **pDPP4T-1** < **pDPP4T-2** < **pDPP4T-3**. These results are consistent with the facts that (i) hole mobilities of **pDPP4T-1**, **pDPP4T-2**, and **pDPP4T-3** are enhanced after thermal annealing at 100 °C, and (ii) they increase in the following order: **pDPP4T-1** < **pDPP4T-2** < **pDPP4T-3** (see Table 2).

The *out-of-plane* diffractions of **pDPP4T-1**, **pDPP4T-2**, and **pDPP4T-3** after thermal annealing at 100 °C were also compared with those of **pDPP4T-A**, **pDPP4T-B**, and **pDPPT-C**, respectively (see Figure S10). The intensities of (100), (200), (300), and (400) diffractions of **pDPP4T-1** are stronger than those of the respective four diffractions of **pDPP4T-A**, respectively. Similarly, **pDPP4T-2** and **pDPP4T-3** show stronger diffractions compared with **pDPP4T-B** and **pDPP4T-C**, respectively. Such comparison clearly manifests that the alkyl chain packing order is improved after incorporation of urea groups in the side chains of these conjugated polymers.[41]

In short, these X-ray diffraction data indicate that the presence of urea groups in the alkyl side chains of these conjugated D−A polymers will not only facilitates the lamellar stacking of alkyl chains, but also does introduce some limited $\pi-\pi$ stacking of neighboring conjugated backbones. This is in good agreement with the observations that (i) hole mobility is enhanced after incorporation of urea groups in the side chains, and (ii) higher hole mobility is measured, especially after annealing, when the side chains contain more urea groups. It also seems to agree with a recent report by Zhang and co-workers that suggests the good charge transport can be obtained in conjugated polymers in absence of a large amount of well-developed $\pi-\pi$ stacks.[42]

AFM Characterization for Thin Films of These Conjugated Polymers. Further structural information were obtained from atomic force microscopy. Figure 5 shows AFM images of the as-prepared thin films of these conjugated polymers before and after thermal annealing at 100 and 120 °C. Compared to **pDPP4T**, **pDPP4T-A**, **pDPP4T-B**, and **pDPP4T-C** (see Figure S11), these polymers with urea groups in the side chains, in particular **pDPP4T-2** and **pDPP4T-3**, were assembled into relatively long and wide nanofibers which are well inter-connected within their thin films. The average widths of nanofibers in thin films of **pDPP4T-1**, **pDPP4T-2**, and **pDPP4T-3** after thermal annealing at 100 °C were measured to be ∼35, ∼45, and ∼50 nm, respectively, whereas the width of nanofibers in thin films of **pDPP4T** was around 30 nm after annealing at 100 °C. Concomitantly, the root-mean-square roughness (R_{RMS}) was found to be slightly higher than

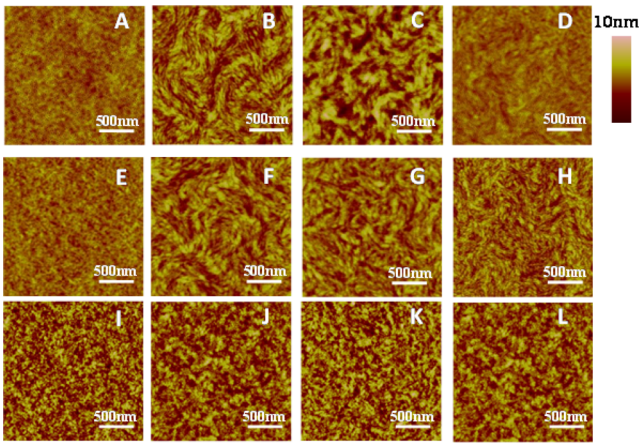

Figure 5. AFM height images of thin films of (A,E,I) **pDPP4T-1**, (B,F,J) **pDPP4T-2**, (C,G,K) **pDPP4T-3**, and (D,H,L) **pDPP4T** deposited on OTS-modified SiO_2/Si substrates (top) at room temperature and after thermal annealing at (middle) 100 °C and (bottom) 120 °C.

for thin films of these conjugated polymers after thermal annealing. For instance, R_{RMS} of thin film of **pDPP4T-3** reached 1.53 nm after thermal annealing at 100 °C. The formation of thick nanofibers is very likely owing to the inter-connection of polymer domains via H-bonding of urea groups in the side chains of these polymers, as illustrated in Scheme 1, and likely being somewhat beneficial for charge transporting on the basis of previous reports.[3d,29a,43] However, nanofibers in thin films of **pDPP4T-1**, **pDPP4T-2**, and **pDPP4T-3** became short and more boundary areas emerged after further thermal annealing at 120 °C. This may be caused by the fact that H-bonding becomes unstable at high temperature. Such morphological change will be detrimental to charge transporting, although the corresponding diffraction intensities increase slightly after further annealing at 120 °C for thin films of **pDPP4T-1**, **pDPP4T-2**, and **pDPP4T-3** (see Figure S7). This agrees with the observation that hole mobilities of **pDPP4T-1**, **pDPP4T-2**, and **pDPP4T-3** started to decrease after further annealing at 120 °C (see Table 2).

Improvement of Photovoltaic Performance. **pDPP4T-1**, **pDPP4T-2**, and **pDPP4T-3** were also utilized as electron donors for photovoltaic devices after blending with $PC_{71}BM$ as the electron acceptor. Blended thin films of these conjugated polymers with $PC_{71}BM$ at different weight ratios were employed as active layers for fabrication of photovoltaic cells with the configuration of ITO/PEDOT:PSS/active layer/Ca/Al (for photovoltaic device fabrication details, see Supporting Information). For comparison, the photovoltaic cells of blends of **pDPP4T-A**, **pDPP4T-B**, **pDPP4T-C**, and **pDPP4T** with $PC_{71}BM$ were fabricated under the same condition. The devices were optimized to maximize the photovoltaic performances by varying the ratios of donor and acceptor and selecting appropriate solvents. Figure 6 shows the $J-V$ curves of photovoltaic cells with the respective blended films of **pDPP4T-1**, **pDPP4T-2**, **pDPP4T-3**, and **pDPP4T** with $PC_{71}BM$ and the corresponding IPCE spectra as well under the respective optimization conditions. The respective $J-V$ curves and IPCE spectra for the blend thin films of **pDPP4T-A**, **pDPP4T-B**, and **pDPP4T-C** with $PC_{71}BM$ are shown in Figure S12.

DOI: 10.1021/jacs.5b09737
J. Am. Chem. Soc. 2016, 138, 173−185

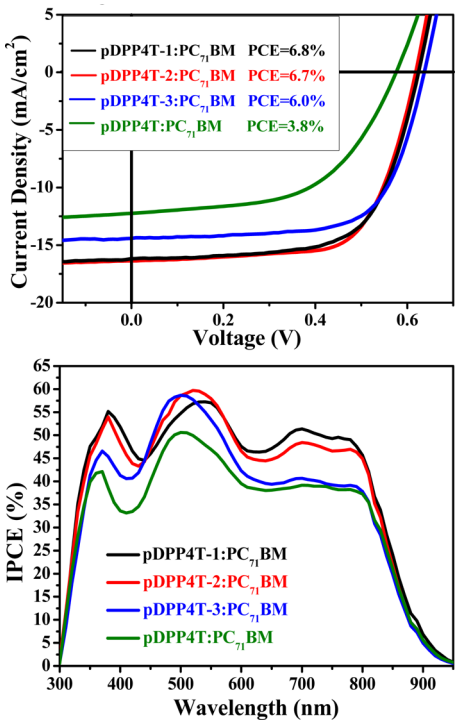

Figure 6. (Top) $J-V$ curves and (bottom) IPCE spectra of photovoltaic cells with the respective blended films of **pDPP4T-1**, **pDPP4T-2**, **pDPP4T-3**, and **pDPP4T** (**pDPP4T**:$PC_{71}BM$, 1:1, w/w) with $PC_{71}BM$ under AM 1.5 illumination (100 mW/cm^2).

As listed in Table 3, the respective blend thin films of **pDPP4T-1**, **pDPP4T-2**, and **pDPP4T-3** with $PC_{71}BM$ exhibit higher PCEs; the PCEs are 6.8%, 6.7%, and 6.0%, respectively, for **pDPP4T-1**, **pDPP4T-2**, and **pDPP4T-3** after blending with $PC_{71}BM$ at a weight ratio of 1:2. The device results are consistent with IPCE spectra as depicted in Figure 6. The IPCE of thin films of **pDPP4T-1**, **pDPP4T-2**, and **pDPP4T-3** with $PC_{71}BM$ can reach 60%, and **pDPP4T-1** and **pDPP4T-2** exhibit higher IPCE than **pDPP4T-3** and **pDPP4T** in the range of 550−800 nm.

We also fabricated the photovoltaic cell using **pDPP4T**:$PC_{71}BM$ (1:1, w/w) as the active layer with the same conditions as reported early, and the PCE was measured to be 3.8%. The maximum PCE was reported to be 5.62% for **pDPP4T**:$PC_{71}BM$ thin film at 1:1 ratio.[44] The relatively low PCE in our study may be owing to the fact the molecular weight (M_w) of **pDPP4T** (40.2 kg mol^{-1}) in our study is lower than that of the polymer (73 kg mol^{-1}) reported in the literature.[44a] The photovoltaic performance of the **pDPP4T**:$PC_{71}BM$ thin film at 1:2 ratio was also tested by using mixed solvent (chloroform/*o*-dichlorobenzene/chloronaphthalene, 100/25/3, v/v/v) as the processing solvent, and the PCE was measured to 3.3% (see Table 3).

In comparison, the maximum PCEs of the blended thin films of **pDPP4T-A**, **pDPP4T-B**, and **pDPP4T-C** with $PC_{71}BM$ each at 1:2 ratios were measured to be 4.8%, 4.8%, and 2.2%, respectively (see Table 3) under optimized conditions. These comparison results clearly reveal that the incorporation of urea groups in the side chains of conjugated D−A polymers such as in **pDPP4T-1**, **pDPP4T-2**, and **pDPP4T-3** is beneficial for improving the photovoltaic performances after blending with $PC_{71}BM$.

In order to establish some structure/property inter-relationships, the surface morphologies of all blended films were characterized with AFM and STEM. On the basis of the AFM height and phase images shown in Figure 7, one may deduce some micro-phase separation, in particular for **pDPP4T-2**:$PC_{71}BM$ and **pDPP4T-3**:$PC_{71}BM$. Clear is that different surface morphologies are obtained when using different donors. The R_{RMS} values of blended films of **pDPP4T-2** and **pDPP4T-3** with $PC_{71}BM$ were measured to be 1.39 and 1.34 nm, respectively. In comparison, the respective blended films of **pDPP4T-1** (0.84 nm) and **pDPP4T** (1.12 nm) with $PC_{71}BM$ show low R_{RMS}. On one hand, high R_{RMS} can imply a fine

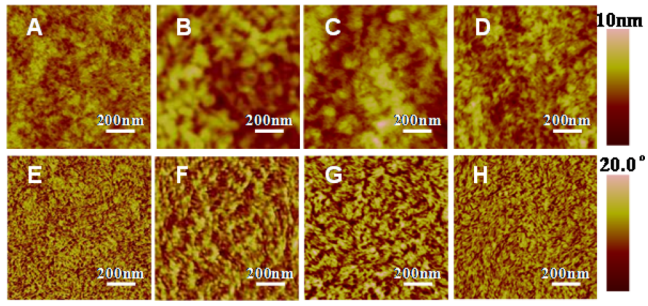

Figure 7. (Top) AFM height and (bottom) phase images of (A,E) **pDPP4T-1**:$PC_{71}BM$, (B,F) **pDPP4T-2**:$PC_{71}BM$, (C,G) **pDPP4T-3**:$PC_{71}BM$, and (D,H) **pDPP4T**:$PC_{71}BM$ (1:1, w/w) blended films.

Table 3. Optimized Photovoltaic Performances of Blends of pDPP4T-1, pDPP4T-2, pDPP4T-3, pDPP4T, pDPP4T-A, pDPP4T-B, and pDPP4T-C with $PC_{71}BM$[a]

donor:acceptor	ratio (w:w)	solvent	V_{oc}(V)	J_{sc}(mA/cm^2)	FF	PCE (%)
pDPP4T-1/$PC_{71}BM$	1:2	CF/*o*-DCB/CN[b]	0.63	16.5	0.65	6.8 (6.5 ± 0.3)
pDPP4T-2/$PC_{71}BM$	1:2	CF/*o*-DCB/CN[c]	0.62	16.3	0.66	6.7 (6.4 ± 0.3)
pDPP4T-3/$PC_{71}BM$	1:2	CF/*o*-DCB/CN[b]	0.63	14.1	0.67	6.0 (5.7 ± 0.3)
pDPP4T-A/$PC_{71}BM$	1:2	CF/*o*-DCB/CN[c]	0.62	12.1	0.61	4.8 (4.6 ± 0.2)
pDPP4T-B/$PC_{71}BM$	1:2	CF/*o*-DCB/CN[c]	0.62	12.1	0.61	4.8 (4.7 ± 0.1)
pDPP4T-C/$PC_{71}BM$	1:2	TCE/CN[d]	0.58	9.3	0.41	2.2(1.9 ± 0.3)
pDPP4T/$PC_{71}BM$	1:2	CF/*o*-DCB/CN[e]	0.58	10.6	0.53	3.3 (3.1 ± 0.2)
pDPP4T/$PC_{71}BM$	1:1	CF/*o*-DCB[f]	0.58	12.3	0.53	3.8 (3.6 ± 0.2)
reference	1:1	CF/*o*-DCB[f]	0.63	14.87	0.60	5.62[max]

[a]The photovoltaic parameters of the best-performing devices are shown. The average values and standard deviations of the PCE are based on more than 10 devices. [b]Devices prepared from mixed solvents chloroform/*o*-dichlorobenzene/chloronaphthalene (100/6/3, v/v/v). [c]Chloroform/*o*-dichlorobenzene/chloronaphthalene (100/4/3, v/v/v). [d]1,1,2,2-Tetrachloroethane/chloronaphthalene (100/3, v/v). [e]Chloroform/*o*-dichlorobenzene/chloronaphthalene (100/25/3, v/v/v). [f]Chloroform/*o*-dichlorobenzene (4/1, v/v).

DOI: 10.1021/jacs.5b09737
J. Am. Chem. Soc. 2016, 138, 173−185

micro-phase separation which is thought of being beneficial for exciton dissociation, thus, for improving the PCE.[45a] On the other hand, low R_{RMS} indicates the smoothness of the blend thin films. According to previous reports,[45] such evenly distributed morphological features may reduce charge recombination.

Figure 8 shows the STEM images of our blended thin films. Light-colored fibril-like structures were detected for blends of

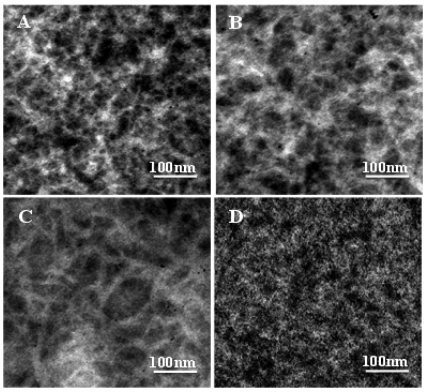

Figure 8. STEM images of (A) **pDPP4T-1**:$PC_{71}BM$, (B) **pDPP4T-2**:$PC_{71}BM$, (C) **pDPP4T-3**:$PC_{71}BM$, and (D) **pDPP4T**:$PC_{71}BM$ (1:1, w/w) blended thin films.

pDPP4T-1, **pDPP4T-2**, and **pDPP4T-3** with $PC_{71}BM$; a higher content of nanofibers were found in **pDPP4T-2**:$PC_{71}BM$ and **pDPP4T-3**:$PC_{71}BM$ thin films. On the basis of previous reports the formation of such nanofibers can be attributed to the assemblies of the donor polymer.[46] The presence of nanofibers within the blending thin films is beneficial for charge transporting. The latter certainly agrees well with the observation that both fill factor (FF) and short-circuit current density (J_{sc}) are enhanced for blended films of **pDPP4T-1**, **pDPP4T-2**, and **pDPP4T-3** with $PC_{71}BM$ in comparison with those of **pDPP4T**:$PC_{71}BM$ thin films (see Table 3). The average width of nanofibers within **pDPP4T-3**:$PC_{71}BM$ thin film was measured to be 20 nm, larger than those of **pDPP4T-2**:$PC_{71}BM$ (11 nm) and **pDPP4T-1**:$PC_{71}BM$ (9 nm) thin films. This may explain the slight reduction of J_{sc} and thus PCE for the photovoltaic cell with **pDPP4T-3**:$PC_{71}BM$ as the active layer since larger nanofibers would be detrimental for exciton diffusion into the donor−-acceptor interface. In comparison, for **pDPP4T**:$PC_{71}BM$ film it is difficult to find a fibril-like morphology (see Figure 8), indicating less phase separation, which is consistent with the relatively feature-less AFM image. This poor phase separation would enhance charge recombination, and thus would result in the observed low FF and J_{sc} (see Table 3).

Finally we also investigated the degree of inter-chain packing of blended thin films using 2D GIXRD. As shown in Figure 9, two diffractions along the q_z direction, corresponding to the (100) and (200) ones, at q_z = 0.33 and 0.65 $Å^{-1}$, were detected for **pDPP4T-1**:$PC_{71}BM$. The corresponding d-spacing was estimated to be 19.05 Å. Similarly, two diffractions at q_z = 0.32 and 0.65 $Å^{-1}$ along the q_z direction, corresponding to a d-spacing of 19.60 Å were observed for **pDPP4T-2**:$PC_{71}BM$; the respective (100) and (200) diffractions at q_z = 0.33 and 0.65 $Å^{-1}$, corresponding to a d-spacing of 19.16 Å, were found for **pDPP4T-3**: $PC_{71}BM$. In comparison, only the (100) diffraction at q_z = 0.31 $Å^{-1}$, corresponding to a d-spacing of 20.54 Å, was detected for the **pDPP4T**: $PC_{71}BM$ thin film. Moreover, the (100) diffraction intensities for the blended thin films of **pDPP4T-1**, **pDPP4T-2**, and **pDPP4T-3** with $PC_{71}BM$ are obviously higher than that of **pDPP4T**:$PC_{71}BM$ (1:1, w/w) thin film. Therefore, it can be concluded that the incorporation of urea group in the alkyl side chains can improve the lamellar packing order for the alkyl chains of these DPP polymers and, therefore, likely induce a micro-phase separation from the fullerene. Indeed, a ring-like diffraction pattern at $q_z \approx 1.31$ $Å^{-1}$ was found for blended thin films of **pDPP4T-1**, **pDPP4T-2**, and **pDPP4T-3** with $PC_{71}BM$. By comparing with the reported data, such ring-like signal is owing to the (311) diffraction of $PC_{71}BM$,[47] suggesting that $PC_{71}BM$ can form ordered aggregates within these blended films. This may be understood as following: the H-bonding owing to the urea groups in the side chains of **pDPP4T-1**, **pDPP4T-2**, and **pDPP4T-3** may facilitate the self-assemblies of these polymers into nanofibers (see Figure 8); as a result, ordered aggregation of molecules of $PC_{71}BM$ occurs within the blended thin films, leading to a micro-phase separation of the two components and facilitating migration of holes and electrons. In addition, a partial arc diffraction (albeit weak and diffused) at $q_z \approx 1.74$ $Å^{-1}$ was observed for **pDPP4T-1**:$PC_{71}BM$ (see Figure 9). The fact that the stronger diffraction intensity of this partial arc signal appears at $q_{xy} \approx 0$ implies that out-of-plane $\pi-\pi$ stacking exists within the **pDPP4T-1**:$PC_{71}BM$ thin films, assisting with charge transport to the respective electrode. To conclude, our GIXRD data agree well with the observation that blends of **pDPP4T-1**, **pDPP4T-2**, and **pDPP4T-3** with $PC_{71}BM$ exhibit higher PCEs, and **pDPP4T-1**:$PC_{71}BM$ shows the highest PCE.

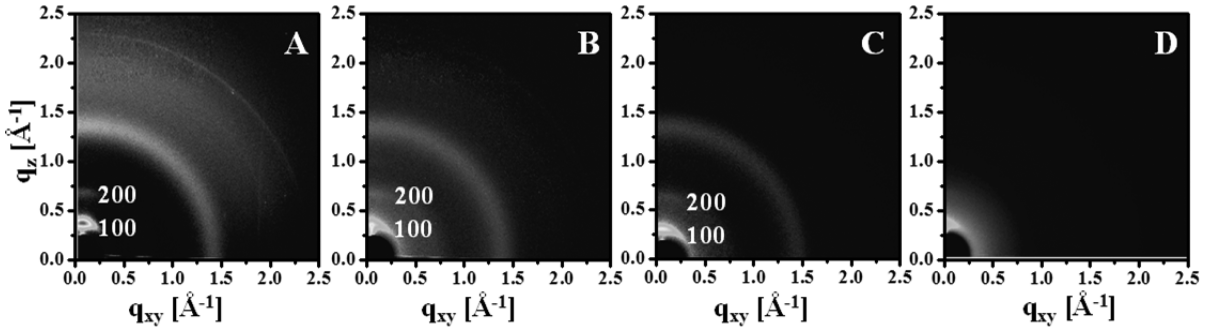

Figure 9. Grazing incidence X-ray diffraction patterns of the blended thin films of (A) **pDPP4T-1**, (B) **pDPP4T-2**, (C) **pDPP4T-3**, and (D) **pDPP4T** with $PC_{71}BM$.

DOI: 10.1021/jacs.5b09737
J. Am. Chem. Soc. 2016, 138, 173−185

CONCLUSIONS

In this article, we report the remarkable enhancement of hole moblities for DPP−quaterthiophene conjugated polymers by incorporating urea groups in the alkyl side chains. Three conjugated polymers **pDPP4T-1**, **pDPP4T-2**, and **pDPP4T-3**, in which the molar ratios of the urea-containing alkyl chains vs branching alkyl chains are 1:30, 1:20, and 1:10, respectively, were prepared and characterized. For comparison, **pDPP4T** without urea groups in the alkyl side chains as well as **pDPP4T-A**, **pDPP4T-B**, and **pDPP4T-C** containing both linear and branched alkyl chains were also prepared. Both IR and ^{1}H NMR spectra data indicate the existence of inter-chain H-bonding for **pDPP4T-1**, **pDPP4T-2**, and **pDPP4T-3**. On the basis of the performances of FETs with thin films of these conjugated polymers, thin films of **pDPP4T-1**, **pDPP4T-2**, and **pDPP4T-3** exhibit higher hole mobilities than those of **pDPP4T-A**, **pDPP4T-B**, **pDPP4T-C**, and **pDPP4T**; thin-film mobility increases in the order **pDPP4T-1**<**pDPP4T-2** < **pDPP4T-3**, and the hole mobility of a thin film of **pDPP4T-3** can reach 13.1 $cm^2\ s^{-1}\ V^{-1}$ after thermal annealing at just 100 °C. It is noted that this is among the highest hole mobilities reported for conjugated polymers so far. Such remarkable enhancement of hole mobility is attributed to the following facts: (i) the lamellar packing order of the alkyl chains is obviously enhanced for thin films of **pDPP4T-1**, **pDPP4T-2**, and **pDPP4T-3**, and (ii) slight inter-chain $\pi-\pi$ stacking emerges for **pDPP4T-2** and **pDPP4T-3** after thermal annealing.

The incorporation of urea groups in the alkyl side chains also has an interesting effect on the photovoltaic performances of DPP−quaterthiophene conjugated polymers after blending with $PC_{71}BM$. The presence of urea groups may facilitate both the assemblies of these conjugated polymers into nanofibers and, as a consequence, the ordered aggregation of $PC_{71}BM$. AFM images indicate some degree of micro-phase separation for **pDPP4T-1**:$PC_{71}BM$, **pDPP4T-2**:$PC_{71}BM$, and **pDPP4T-3**:$PC_{71}BM$. The variations of inter-chain packing and thin-film morphology result in the improvement of PCEs for the blended films of these conjugated polymers entailing urea groups with $PC_{71}BM$ by comparing with those of **pDPP4T**:$PC_{71}BM$, **pDPP4T-A**:$PC_{71}BM$, **pDPP4T-B**:$PC_{71}BM$, and **pDPP4T-C**:$PC_{71}BM$. Among these blend thin films, **pDPP4T-1**: $PC_{71}BM$ exhibits the highest PCE up to 6.8%. The PCE of the photovoltaic cell with the **pDPP4T-3**: $PC_{71}BM$ thin film is slightly reduced. Overall, our data demonstrates that side chain engineering via hydrogen-bonding (through the incorporation of urea groups) is a powerful strategy to improve the charge carrier mobilities and photovoltaic performance for conjugated polymers and likely can be applied to other conjugated polymers. Thereby, other functional moieties besides urea moiety may be incorporated into the alkyl side chains of conjugated polymers to tune the inter-chain interactions/packing and thus further improve their semiconducting performance, providing a whole library of options to further develop this interesting class of semiconductors.

EXPERIMENTAL SECTION

Materials and Characterization Techniques. The reagents and starting materials were commercially available and used without any further purification, if not specified elsewhere.

^{1}H NMR and ^{13}C NMR spectra were recorded on Bruker AVANCE III 500, 400, and 300 MHz spectrometers. Elemental analysis was performed on a Carlo Erba model 1160 elemental analyzer. UV−vis absorption spectra were measured with JASCO V-570 UV−vis spectrophotometer. IR spectra were recorded on a JASCO FT/IR-480 plus Fourier transform infrared spectrometer. Gel permeation chromatography (GPC) analysis was performed on an PL-GPC 220 high-temperature chromatograph at 150 °C equipped with a IR5 detector; polystyrene was used as the calibration standard and 1,2,4-trichlorobenzene as eluent; the flow rate was 1.0 mL/min. Thermogravimetric analysis (TGA) were carried out on a Shimadzu DTG-60 instruments under a dry nitrogen flow; the heating was carried out from room temperature to 550 °C with a heating rate of 10 °C/min. For differential scanning calorimetry (DSC) measurements, ∼3 mg of material was used; the measurements were conducted under nitrogen at a scan rate of 10 °C/min with a DSC-Q2000 instrument. Cyclic voltammetric measurements were carried out in a conventional three-electrode cell using a glassy carbon working electrode, a Pt counter electrode, and a Ag/AgCl (saturated KCl) reference electrode on a computer-controlled CHI660C instruments at room temperature; the scan rate was 100 mV s^{-1}, and n-Bu_4NPF_6 (0.1 M) was used as the supporting electrolyte. Thin-film thickness of all copolymers was measured on a profilometer (Ambios Tech. XP-2). The GIXRD data were obtained at beam line BL14B1 of the Shanghai Synchrotron Radiation Facility (SSRF) and 1W1A of the Beijing Synchrotron Radiation Facility for 1D diffraction profiles. The thin-film surfaces were examined by tapping-mode AFM using Digital Instruments Nanoscope V atomic force microscope under ambient conditions in the dark. The thin-film morphology was studied with SEM (SU 8020, Hitachi) operating at 25 kV of acceleration voltage in STEM mode. FETs and photovoltaic cells were fabricated following conventional procedures, and the details are provided in the Supporting Information.

*2,5-Bis(6-azidohexyl)-3,6-bis(5-bromothiophen-2-yl)pyrrolo[3,4-c]pyrrole-1,4(2H,5H)-dione (**5**).* 2,5-Bis(6-bromohexyl)-3,6-bis(5-bromothiophen-2-yl)pyrrolo[3,4-*c*]pyrrole-1,4(2*H*,5*H*)-dione (1.0 g, 1.28 mmol) was dissolved in 200 mL of tetrahydrofuran. Sodium azide (249.6 mg, 3.84 mmol) dissolved in 10 mL of deionized water was added. The reaction mixture was heated to 70 °C and stirred 48 h. After cooling down to room temperature, the solvent was removed under reduced pressure. The residue was dissolved in CH_2Cl_2 and washed with 100 mL of water three times. The organic phase was dried over $MgSO_4$ and filtered. The filtrate was then concentrated under reduced pressure. The crude product was purified by column chromatography with petroleum ether (60−90 °C) and CH_2Cl_2 (1:1, v/v) as the eluent. Compound **5** was obtained as dark red solids (403.8 mg, 45%). ^{1}H NMR ($CDCl_3$, 300 MHz): δ 8.67 (d, 2H, J = 3.9 Hz), 7.25 (d, 2H, J = 6.0 Hz), 4.00 (t, 4H, J = 7.5 Hz), 3.27 (t, 4H, J = 6.8 Hz), 1.74 (m, 4H), 1.61 (m, 4H), 1.44 (m, 8H). ^{13}C NMR ($CDCl_3$; 100 MHz): δ 161.20, 139.13, 135.77, 131.95, 131.20, 119.60, 108.15, 51.58, 42.23, 30.14, 28.99, 26.65, 26.61. MS (MALDI-TOF): 708.1 $[M]^+$. Anal. Calcd for $C_{26}H_{28}Br_2N_8O_2S_2$: C, 44.08; H, 3.98; N, 15.82; S, 9.05. Found: C, 43.95; H, 4.03; N, 15.64; S, 9.31.

*2,5-Bis(6-aminohexyl)-3,6-bis(5-bromothiophen-2-yl)pyrrolo[3,4-c]pyrrole-1,4(2H,5H)-dione (**6**).* Compound **5** (403.8 mg, 0.57 mmol), triphenylphosphine (897.0 mg, 3.42 mmol), deionized water (102.6 μL, 5.70 mmol) was dissolved in 150 mL of toluene. The reaction mixture was heated to 80 °C and stirred overnight under N_2 atomosphere. After cooling down to room temperature, 200 mL of ethanol was added and filtered, then washed with 100 mL of ethanol and 100 mL of $CHCl_3$ for three times. Compound **6** was obtained as dark red solids (256.0 mg, 68%). Compound **6** was used directly without further purifications. MS (MALDI-TOF): 657.0 $[M+H]^+$.

*1,1′-((3,6-Bis(5-bromothiophen-2-yl)-1,4-dioxopyrrolo[3,4-c]-pyrrole-2,5(1H,4H)-diyl)bis(hexane-6,1-diyl))bis(3-hexylurea) (**1**).* Compound **6** (256.4 mg, 0.39 mmol) and hexyl isocyanate (148.8 mg, 1.17 mol) were dissolved in 100 mL of $CHCl_3$. The reaction mixture was heated to 80 °C and stirred overnight under N_2 atomosphere. After cooling down to room temperature, the solvent was removed and the crude product was recrystallized from $CHCl_3$ for three times. Compound 1 was obtained as dark red solids (209.5 mg, 59%). ^{1}H NMR (500 MHz, 1,1,2,2-tetrachloroethane-d_2, 100 °C): δ

DOI: 10.1021/jacs.5b09737
J. Am. Chem. Soc. 2016, 138, 173−185

8.49 (d, 2H, J = 4.0 Hz), 7.25 (d, 2H, J = 4.0 Hz), 5.14 (s, br, 4H), 3.99 (t, 4H, J = 7.5 Hz), 3.13 (q, 8H, J = 7.0 Hz), 2.19 (m, 2H), 2.05 (d, 2H, J = 5.0 Hz), 1.76 (m, 4H), 1.50−1.30 (m, 24H), 0.91 (t, 6H, J = 6.5 Hz). ^{13}C NMR (100 MHz, solid): 159.25, 137.07, 134.02, 130.68, 118.31, 109.42, 106.09, 41.21, 27.70. MS (MALDI-TOF): 933.4 $[M+Na]^+$. Anal. Calcd for $C_{40}H_{58}Br_2N_6O_4S_2$: C, 52.74; H, 6.42; N, 9.23; S, 7.04. Found: C, 52.64; H, 6.60; N, 8.99; S, 6.94.

General Synthetic Procedures for pDPP4T-1, pDPP4T-2, and pDPP4T-3. Monomer **1** (x mol), 3,6-bis(5-bromothiophen-2-yl)-2,5-bis(2-octyldodecyl)pyrrolo[3,4-c]pyrrole-1,4(2H,5H)-dione (**2**) (y mol), 5,5′-bis(trimethylstannyl)-2,2′-bithiophene (**3**) [1 equiv based on (x + y) mol] and P(o-tol)$_3$ (0.16 equiv) were dissolved in toluene (10 mL). The solution was purged with N_2 for 30 min, followed by addition of $Pd_2(dba)_3$ (0.02 equiv). The reaction mixture was stirred at 100 °C for 72 h. The resulting mixture was poured into methanol and stirred for 3.0 h. The dark precipitate was filtered off and subjected to Soxhlet extraction for 2 days successively with methanol, hexane, and acetone to remove oligomers and the remaining catalyst. The resulting polymer was extracted with chloroform and precipitated again from methanol, filtered, washed with methanol, and dried under vacuum at 50 °C for 48 h.

Synthesis of ***pDPP4T-1****.* Compound **1** (3.0 mg, 0.0033 mmol), compound **2** (101.9 mg, 0.10 mmol), compound **3** (50.7 mg, 0.10 mmol), P(o-tol)$_3$ (5.0 mg, 0.016 mmol), and $Pd_2(dba)_3$ (1.9 mg, 0.0021 mmol) were used. The purified polymer was collected to give deep green solid (86.1 mg, 82% yield). ^{1}H NMR (500 MHz, 1,1,2,2-tetrachloroethane-d_2, 80 °C): δ 8.97−8.87 (m, br, 2H), 7.32−6.98 (m, br, 6H), 5.21 (s, br, 0.13H), 407−3.93 (m, br, 4H), 2.23−2.05 (m, br, 10H), 1.51−1.31 (m, br, 56H), 0.92 (s, 12H). ^{13}C NMR (100 MHz, solid): δ 160.20, 140.12, 136.25, 128.15, 123.68, 108.04, 45.08, 38.45, 30.29, 23.14, 14.49. M_w/M_n (GPC) = 75.6/28.4 kg mol^{-1}. Anal. Calcd for $(C_{1908}H_{2762}N_{66}O_{64}S_{124})_n$: C, 72.46; H, 8.80; N, 2.92; S, 12.57. Found: C, 72.23; H, 8.92; N, 2.95; S, 12.43.

Synthesis of ***pDPP4T-2****.* Compound **1** (4.6 mg, 0.0050 mmol), compound **2** (101.9 mg, 0.10 mmol), compound **3** (51.8 mg, 0.11 mmol), P(o-tol)$_3$ (5.1 mg, 0.017 mmol), and $Pd_2(dba)_3$ (1.9 mg, 0.0021 mmol) were used. The purified polymer was collected to give deep green solid (88.0 mg, 82% yield). ^{1}H NMR (500 MHz, 1,1,2,2-tetrachloroethane-d_2, 100 °C): δ 8.94−8.84 (m, br, 2H), 7.38−7.00 (m, br, 6H), 5.16 (s, br, 0.19H), 4.09 (s, br, 4H), 2.06 (m, br, 10H), 1.46−1.33 (m, br, 56H), 0.94−0.93 (m, br, 12H). ^{13}C NMR (100 MHz, solid): δ 160.10, 140.27, 136.18, 128.10, 123.62, 107.94, 44.86, 38.41, 30.16, 23.04, 14.40. M_w/M_n (GPC) = 46.2/19.8 kg mol^{-1}. Anal. Calcd for $(C_{1288}H_{1862}N_{46}O_{44}S_{84})_n$: C, 72.33; H, 8.77; N, 3.01; S, 12.59. Found: C, 72.11; H, 8.67; N, 2.93; S, 12.44.

Synthesis of ***pDPP4T-3****.* Compound **1** (9.1 mg, 0.010 mmol), compound **2**(101.9 mg, 0.10 mmol), compound **3** (54.1 mg, 0.11 mmol), P(o-tol)$_3$ (5.4 mg, 0.018 mmol), and $Pd_2(dba)_3$ (2.0 mg, 0.0022 mmol) were used. The purified polymer was collected to give deep green solid (91.2 mg, 81% yield). ^{1}H NMR (500 MHz, 1,1,2,2-tetrachloroethane-d_2, 80 °C): δ 8.97−8.76 (m, br, 2H), 7.37−6.98 (m, br, 6H), 5.21 (s, br, 0.36H), 4.07 (s, br, 4H), 2.18−2.05 (m, br, 10H), 1.51−1.31 (m, br, 56H), 0.92 (s, 12H). ^{13}C NMR (100 MHz, solid): δ 160.15, 140.07, 136.20, 128.10, 123.63, 107.99, 45.03, 38.40, 30.24, 23.09, 14.44. M_w/M_n (GPC) = 42.2/16.6 kg mol^{-1}. Anal. Calcd for $(C_{668}H_{962}N_{26}O_{24}S_{44})_n$: C, 71.94; H, 8.69; N, 3.27; S, 12.65. Found: C, 72.16; H, 8.48; N, 3.05; S, 12.68.

■ ASSOCIATED CONTENT

Supporting Information

The Supporting Information is available free of charge on the ACS Publications website at DOI: 10.1021/jacs.5b09737.

TGA, DSC, cyclic voltammograms, synthesis of **pDPP4T**, **pDPP4T-A**, **pDPP4T-B**, and **pDPP4T-C**, HOMO/LUMO energies and band gaps of **pDPP4T-A**, **pDPP4T-B**, and **pDPP4T-C**, fabrication of BGBC and BGTC FETs, device characterization and stability, 1D X-ray diffraction patterns, AFM images of **pDPP4T-A**, **pDPP4T-B**, and **pDPP4T-C**, fabrication of photovoltaic cells, J−V curves and IPCE spectra of **pDPP4T-A**, **pDPP4T-B**, and **pDPP4T-C**, and ^{1}H NMR and ^{13}C NMR spectra, including Figures S1−S12 and Tables S1 and S2 (PDF)

■ AUTHOR INFORMATION

Corresponding Authors

* drzitong@gmail.com

*dqzhang@iccas.ac.cn

Present Address

†D.Z.: Beijing National Laboratory for Molecular Sciences, Organic Solids Laboratory, Institute of Chemistry, Chinese Academy of Sciences, Beijing 100190, China

Notes

The authors declare no competing financial interest.

■ ACKNOWLEDGMENTS

The present research was financially supported by NSFC (21190032, 21372226) and the Strategic Priority Research Program of the Chinese Academy of Sciences (XDB12010300). The authors thank Prof. Yongfang Li for allowance for using the facility for fabrication of OPVs. The authors also thank beamline of BL14B1 of the Shanghai Synchrotron Radiation Facility (SSRF) for providing the beam line, and 1W1A of Beijing Synchrotron Radiation Facility for providing the beam line for 1D diffraction profiles.

■ REFERENCES

(1) (a) Murphy, A. R.; Fréchet, J. M. J. *Chem. Rev.* **2007**, *107*, 1066. (b) Schmidt, R.; Oh, J. H.; Sun, Y.-S.; Deppisch, M.; Krause, A.-M.; Radacki, K.; Braunschweig, H.; Könemann, M.; Erk, P.; Bao, Z. N.; Würthner, F. *J. Am. Chem. Soc.* **2009**, *131*, 6215. (c) Li, L.; Gao, P.; Schuermann, K. C.; Ostendorp, S.; Wang, W.; Du, C.; Lei, Y.; Fuchs, H.; De Cola, L.; Müllen, K.; Chi, L. F. *J. Am. Chem. Soc.* **2010**, *132*, 8807.

(2) (a) Cao, Y.; Steigerwald, M. L.; Nuckolls, C.; Guo, X. F. *Adv. Mater.* **2010**, *22*, 20. (b) Anthony, J. E.; Facchetti, A.; Heeney, M.; Marder, S. R.; Zhan, X. W. *Adv. Mater.* **2010**, *22*, 3876.

(3) (a) Liu, Y.-Y.; Song, C.-L.; Zeng, W.-J.; Zhou, K.-G.; Shi, Z.-F.; Ma, C.-B.; Yang, F.; Zhang, H.-L.; Gong, X. *J. Am. Chem. Soc.* **2010**, *132*, 16349. (b) Liang, Z.; Tang, Q.; Mao, R.; Liu, D.; Xu, J.; Miao, Q. *Adv. Mater.* **2011**, *23*, 5514. (c) Liu, Z. T.; Zhang, G. X.; Cai, Z. X.; Chen, X.; Luo, H. W.; Li, Y. H.; Wang, J. G.; Zhang, D. Q. *Adv. Mater.* **2014**, *26*, 6965. (d) Sirringhaus, H. *Adv. Mater.* **2014**, *26*, 1319.

(4) (a) Zhu, X.; Tsuji, H.; Navarrete, J. T. L.; Casado, J.; Nakamura, E. *J. Am. Chem. Soc.* **2012**, *134*, 19254. (b) Wang, C.; Dong, H.; Hu, W. P.; Liu, Y. Q.; Zhu, D. B. *Chem. Rev.* **2012**, *112*, 2208. (c) Rochat, S.; Swager, T. M. *J. Am. Chem. Soc.* **2013**, *135*, 17703. (d) Bayn, A.; Feng, X. L.; Müllen, K.; Haick, H. *ACS Appl. Mater. Interfaces* **2013**, *5*, 3431. (e) Sukegawa, J.; Schubert, C.; Zhu, X. Z.; Tsuji, H.; Guldi, D. M.; Nakamura, E. *Nat. Chem.* **2014**, *6*, 899.

(5) (a) Takeda, Y.; Andrew, T.; Lobez, J.; Mork, A.; Swager, T. M. *Angew. Chem., Int. Ed.* **2012**, *51*, 9042. (b) Pang, S.; Yang, S.; Feng, X. L.; Müllen, K. *Adv. Mater.* **2012**, *24*, 1566. (c) Li, L.; Gao, P.; Baumgarten, M.; Müllen, K.; Lu, N.; Fuchs, H.; Chi, L. F. *Adv. Mater.* **2013**, *25*, 3419. (d) He, T.; Stolte, M.; Würthner, F. *Adv. Mater.* **2013**, *25*, 6951.

(6) (a) Scarongella, M.; De Jonghe-Risse, J.; Buchaca-Domingo, E.; Causa, M.; Fei, Z.; Heeney, M.; Moser, J.-E.; Stingelin, N.; Banerji, N. *J. Am. Chem. Soc.* **2015**, *137*, 2908. (b) Lin, Y. Z.; Wang, J. Y.; Zhang, Z.-G.; Bai, H. T.; Li, Y. F.; Zhu, D. B.; Zhan, X. W. *Adv. Mater.* **2015**, *27*, 1170. (c) Li, G.; Zhu, R.; Yang, Y. *Nat. Photonics* **2012**, *6*, 153. (d) Liang, Y. Y.; Wu, Y.; Feng, D. Q.; Tsai, S.-T.; Son, H.-J.; Li, G.; Yu, L. P. *J. Am. Chem. Soc.* **2009**, *131*, 56.

DOI: 10.1021/jacs.5b09737
J. Am. Chem. Soc. 2016, 138, 173−185

(7) (a) Buchaca-Domingo, E.; Vandewal, K.; Fei, Z.; Watkins, S. E.; Scholes, F. H.; Bannock, J. H.; de Mello, J. C.; Richter, L. J.; Delongchamp, D. M.; Amassian, A.; Heeney, M.; Salleo, A.; Stingelin, N. *J. Am. Chem. Soc.* **2015**, *137*, 5256. (b) Pang, S.; Hernandez, Y.; Feng, X. L.; Müllen, K. *Adv. Mater.* **2011**, *23*, 2779. (c) Yip, H.-L.; Jen, A. K.-Y. *Energy Environ. Sci.* **2012**, *5*, 5994. (d) Li, Y. F. *Acc. Chem. Res.* **2012**, *45*, 723.
(8) (a) Hou, J. H.; Chen, H.-Y.; Zhang, S. Q.; Chen, R. I.; Yang, Y.; Wu, Y.; Li, G. *J. Am. Chem. Soc.* **2009**, *131*, 15586. (b) Li, K.; Li, Z.; Feng, K.; Xu, X.; Wang, L.; Peng, Q. *J. Am. Chem. Soc.* **2013**, *135*, 13549.
(9) (a) Cheng, Y.-J.; Yang, S.-H.; Hsu, C.-S. *Chem. Rev.* **2009**, *109*, 5868. (b) Ye, L.; Zhang, S. Q.; Huo, L. J.; Zhang, M. J.; Hou, J. H. *Acc. Chem. Res.* **2014**, *47*, 1595.
(10) Johnson, K.; Huang, Y.-S.; Huettner, S.; Sommer, M.; Brinkmann; Mulherin, R.; Niedzialek, D.; Beljonne, D.; Clark, J.; Huck, W. T. S.; Friend, R. H. *J. Am. Chem. Soc.* **2013**, *135*, 5074.
(11) (a) Müllen, K.; Pisula, W. *J. Am. Chem. Soc.* **2015**, *137*, 9503. (b) Bao, Z. N.; Chan, W. K.; Yu, L. P. *J. Am. Chem. Soc.* **1995**, *117*, 12426.
(12) Han, A.-R.; Dutta, G. K.; Lee, J.; Lee, H. R.; Lee, S. M.; Ahn, H.; Shin, T. J.; Oh, J. H.; Yang, C. *Adv. Funct. Mater.* **2015**, *25*, 247.
(13) Kang, I.; Yun, H.-J.; Chung, D. S.; Kwon, S.-K.; Kim, Y.-H. *J. Am. Chem. Soc.* **2013**, *135*, 14896.
(14) Kim, G.; Kang, S.-J.; Dutta, G. K.; Han, Y.-K.; Shin, T. J.; Noh, Y.-Y.; Yang, C. *J. Am. Chem. Soc.* **2014**, *136*, 9477.
(15) (a) Heeger, A. J. *Chem. Soc. Rev.* **2010**, *39*, 2354. (b) Yuen, J. D.; Wudl, F. *Energy Environ. Sci.* **2013**, *6*, 392.
(16) Sun, B.; Hong, W.; Yan, Z. Q.; Aziz, H.; Li, Y. N. *Adv. Mater.* **2014**, *26*, 2636.
(17) (a) Guo, X.; Zhou, N.; Lou, S. J.; Hennek, J. W.; Ortiz, R. P.; Butler, M. R.; Boudreault, P.-L. T.; Strzalka, J.; Morin, P.-O.; Leclerc, M.; Navarrete, J. T. L.; Ratner, M. A.; Chen, L. X.; Chang, R. P. H.; Facchetti, A.; Marks, T. J. *J. Am. Chem. Soc.* **2012**, *134*, 18427. (b) Guo, X.; Facchetti, A.; Marks, T. J. *Chem. Rev.* **2014**, *114*, 8943.
(18) (a) Wang, M.; Wang, H.; Yokoyama, T.; Liu, X.; Huang, Y.; Zhang, Y.; Nguyen, T.-Q.; Aramaki, S.; Bazan, G. C. *J. Am. Chem. Soc.* **2014**, *136*, 12576. (b) Liu, X.; Hsu, B. B. Y.; Sun, Y. M.; Mai, K.-K.; Heeger, A. J.; Bazan, G. C. *J. Am. Chem. Soc.* **2014**, *136*, 16144.
(19) Stuart, A. C.; Tumbleston, J. R.; Zhou, H.; Li, W.; Liu, S.; Ade, H.; You, W. *J. Am. Chem. Soc.* **2013**, *135*, 1806.
(20) Li, Y. N.; Sonar, P.; Murphy, L.; Hong, W. *Energy Environ. Sci.* **2013**, *6*, 1684.
(21) (a) Lee, J.; Han, A.-R.; Kim, J.; Kim, Y.; Oh, J. K.; Yang, C. *J. Am. Chem. Soc.* **2012**, *134*, 20713. (b) Zhao, Y.; Guo, Y. L.; Liu, Y. Q. *Adv. Mater.* **2013**, *25*, 5372.
(22) (a) Qin, T.; Zajaczkowski, W.; Pisula, W.; Baumgarten, M.; Chen, M.; Gao, M.; Wilson, G.; Easton, C. D.; Müllen, K.; Watkins, S. E. *J. Am. Chem. Soc.* **2014**, *136*, 6049. (b) Steckler, T. T.; Henriksson, P.; Mollinger, S.; Lundin, A.; Salleo, A.; Andersson, M. R. *J. Am. Chem. Soc.* **2014**, *136*, 1190.
(23) (a) Li, K.; Li, Z.; Feng, K.; Xu, X.; Wang, L.; Peng, Q. *J. Am. Chem. Soc.* **2013**, *135*, 13549. (b) Earmme, T.; Hwang, Y.-J.; Murari, N. M.; Subramaniyan, S.; Jenekhe, S. A. *J. Am. Chem. Soc.* **2013**, *135*, 14960.
(24) (a) He, Z. C.; Xiao, B.; Liu, F.; Wu, H. B.; Yang, Y. L.; Xiao, S.; Wang, C.; Russell, T. P.; Cao, Y. *Nat. Photonics* **2015**, *9*, 174. (b) You, J. B.; Dou, L. T.; Yoshimura, K.; Kato, T.; Ohya, K.; Moriarty, T.; Emery, K.; Chen, C.-C.; Gao, J.; Li, G.; Yang, Y. *Nat. Commun.* **2013**, *4*, 1446. (c) Liu, Y. H.; Zhao, J. B.; Li, Z. K.; Mu, C.; Ma, W.; Hu, H. W.; Jiang, K.; Lin, H. R.; Ade, H.; Yan, H. *Nat. Commun.* **2014**, *5*, 5293. (d) Chen, C.-C.; Chang, W.-H.; Yoshimura, K.; Ohya, K.; You, J. B.; Gao, J.; Hong, Z. R.; Yang, Y. *Adv. Mater.* **2014**, *26*, 5670.
(25) (a) Lu, L. Y.; Yu, L. P. *Adv. Mater.* **2014**, *26*, 4413. (b) Lu, L. Y.; Zheng, T. Y.; Wu, Q. H.; Schneider, A. M.; Zhao, D. L.; Yu, L. P. *Chem. Rev.* **2015**, *115*, 12666.
(26) (a) Mori, D.; Benten, H.; Okada, I.; Ohkita, H.; Ito, S. *Energy Environ. Sci.* **2014**, *7*, 2939. (b) Facchetti, A. *Mater. Today* **2013**, *16*, 123. (c) Earmme, T.; Hwang, Y.-J.; Subramaniyan, S.; Jenekhe, S. A. *Adv. Mater.* **2014**, *26*, 6080.
(27) Lee, J.; Han, A.-R.; Yu, H.; Shin, T. J.; Yang, C.; Oh, J. K. *J. Am. Chem. Soc.* **2013**, *135*, 9540.
(28) (a) Jackson, N. E.; Savoie, B. M.; Kohlstedt, K. L.; de la Cruz, M. O.; Schatz, G. C.; Chen, L. X.; Ratner, M. A. *J. Am. Chem. Soc.* **2013**, *135*, 10475. (b) Jackson, N. E.; Kohlstedt, K. L.; Savoie, B. M.; de la Cruz, M. O.; Schatz, G. C.; Chen, L. X.; Ratner, M. A. *J. Am. Chem. Soc.* **2015**, *137*, 6254.
(29) (a) Lei, T.; Wang, J.-Y.; Pei, J. *Chem. Mater.* **2014**, *26*, 594. (b) Mei, J. G.; Bao, Z. N. *Chem. Mater.* **2014**, *26*, 604. (c) McCulloch, I.; Ashraf, R. S.; Biniek, L.; Bronstein, H.; Combe, C.; Donaghey, J. E.; James, D. I.; Nielsen, C. B.; Schroeder, B. C.; Zhang, W. M. *Acc. Chem. Res.* **2012**, *45*, 714.
(30) Lei, T.; Dou, J.-H.; Pei, J. *Adv. Mater.* **2012**, *24*, 6457.
(31) (a) Yiu, A. T.; Beaujuge, P. M.; Lee, O. P.; Woo, C. H.; Toney, M. F.; Fréchet, J. M. J. *J. Am. Chem. Soc.* **2012**, *134*, 2180. (b) Chen, M. S.; Lee, O. P.; Niskala, J. R.; Yiu, A. T.; Tassone, C. J.; Schmidt, K.; Beaujuge, P. M.; Onishi, S. S.; Toney, M. F.; Zettl, A.; Fréchet, J. M. J. *J. Am. Chem. Soc.* **2013**, *135*, 19229.
(32) (a) Li, Y. N.; Sonar, P.; Singh, S. P.; Soh, M. S.; Van Meurs, M.; Tan, J. *J. Am. Chem. Soc.* **2011**, *133*, 2198. (b) Lei, T.; Dou, J.-H.; Ma, Z.-J.; Yao, C.-H.; Liu, C.-J.; Wang, J.-Y.; Pei, J. *J. Am. Chem. Soc.* **2012**, *134*, 20025. (c) Lei, T.; Xia, X.; Wang, J.-Y.; Liu, C.-J.; Pei, J. *J. Am. Chem. Soc.* **2014**, *136*, 2135. (d) Cai, Z. X.; Luo, H. W.; Qi, P. L.; Wang, J. G.; Zhang, G. X.; Liu, Z. T.; Zhang, D. Q. *Macromolecules* **2014**, *47*, 2899.
(33) We note that the transfer characteristics is not ideal and typically exhibits a region of higher slope at low gate voltage and a region of smaller slope at high gate voltage. Similar non-ideal electrical characteristics have been observed for **pDPP4T**[32a,34] and other DPP-based copolymers[27,35] and its origin currently is not clearly understood. Such bending phenomenon observed for the transfer curves may be due to the carrier super saturation in the conduction channel at high source/drain current regimes or low-density shallow charge trapping in the interfaces.[3d,35a]
(34) (a) Ha, J. S.; Kim, K. H.; Choi, D. H. *J. Am. Chem. Soc.* **2011**, *133*, 10364. (b) Sun, B.; Hong, W.; Aziz, H.; Abukhdeir, N. M.; Li, Y. N. *J. Mater. Chem. C* **2013**, *1*, 4423. (c) Chen, S.; Sun, B.; Hong, W.; Aziz, H.; Meng, Y.; Li, Y. N. *J. Mater. Chem. C* **2014**, *2*, 2183. (d) Hong, W.; Chen, S.; Sun, B.; Arnould, M.; Meng, Y.; Li, Y. N. *Chem. Sci.* **2015**, *6*, 3225.
(35) (a) Li, J.; Zhao, Y.; Tan, H. S.; Guo, Y. L.; Di, C.-A.; Yu, G.; Liu, Y. Q.; Lin, M.; Lim, S. H.; Zhou, Y.; Su, H.; Ong, B. S. *Sci. Rep.* **2012**, *2*, 754. (b) Chen, H. J.; Guo, Y. L.; Yu, G.; Zhao, Y.; Zhang, J.; Gao, D.; Liu, H. T.; Liu, Y. Q. *Adv. Mater.* **2012**, *24*, 4618. (c) Kang, I.; An, T. K.; Hong, J.-a.; Yun, H.-J.; Kim, R.; Chung, D. S.; Park, C. E.; Kim, Y.-H.; Kwon, S.-K. *Adv. Mater.* **2013**, *25*, 524. (d) Matthews, J. R.; Niu, W.; Tandia, A.; Wallace, A. L.; Hu, J.; Lee, W.-Y.; Giri, G.; Mannsfeld, S. C. B.; Xie, Y. T.; Cai, S. C.; Fong, H. H.; Bao, Z. N.; He, M. Q. *Chem. Mater.* **2013**, *25*, 782.
(36) Li and co-workers reported a hole mobility of 5.5 $cm^2 V^{-1} s^{-1}$ for a thin film of **pDPP4T** after thermal annelaing at 200 °C.[34d] Such difference in hole mobility can be interpreted by the following facts: (i) the **pDPP4T** sample used in Li's studies possessed a molecular weight (M_n) of 40 kg mol^{-1} while the molecular weight of the sample employed in our studies was measured to be 18.8 kg mol^{-1}; (ii) the thin films were thermally annealed at different temperatures.
(37) Zhang, M.; Tsao, H. N.; Pisula, W.; Yang, C.; Mishra, A. K.; Müllen. *J. Am. Chem. Soc.* **2007**, *129*, 3472.
(38) We observe that hole mobilities of **pDPP4T-1**, **pDPP4T-2** and **pDPP4T-3** as well as those of **pDPP4T-A**, **pDPP4T-B** and **pDPP4T-C**, which were deduced from the characteristics of BGTC devices, are lower than their corresponding hole mobilities on the basis of the data of the BGBC devices. Similar results were reported for DPP-based conjugated D−A polymer and other organic semiconductors previously.[35a,39] The reason for such phenomenon is still not clear. The vapor-phase evaporation of the metal electrodes in the BGTC

DOI: 10.1021/jacs.5b09737
J. Am. Chem. Soc. 2016, 138, 173−185

structure may damage the semiconducting layer, which will affect the device performance.

(39) (a) Guo, X.; Kim, F. S.; Jenekhe, S. A.; Watson, M. D. *Chem. Mater.* **2012**, *24*, 1434. (b) Ie, Y.; Ueta, M.; Nitani, M.; Tohnai, N.; Miyata, M.; Tada, H.; Aso, Y. *Chem. Mater.* **2012**, *24*, 3285. (c) Zhang, F.; Hu, Y.; Schuettfort, T.; Di, C.-A.; Gao, X.; McNeill, C. R.; Thomsen, L.; Mannsfeld, S. C. B.; Yuan, W.; Sirringhaus, H.; Zhu, D. *J. Am. Chem. Soc.* **2013**, *135*, 2338. (d) Gao, X.; Zhao, Z. *Sci. China: Chem.* **2015**, *58*, 947.

(40) Broad diffractions at $q_{xy} \approx 1.68$ Å^{-1} were also observed for **pDPP4T-1**, **pDPP4T-2**, and **pDPP4T-3** in the 1D diffraction profiles for the in-plane direction (see Figure S8). But, the diffraction for **pDPP4T-1** was rather weak. This agrees well with their 2D GIXRD patterns (see Figure 4).

(41) In addition, the diffractions of **pDPP4T-1**, **pDPP4T-2** and **pDPP4T-3** are sharper, especially for the (100) ones, in comparison with those of **pDPP4T-A**, **pDPP4T-B** and **pDPPT-C**. For instance, the full width at half-maximum (fwhm) of the (100) diffraction of **pDPP4T-3** is 0.66 Å^{-1}, which is smaller than that of **pDPP4T-C** (fwhm = 0.86 Å^{-1}). This implies that ordered and larger molecular domains are formed within thin films of **pDPP4T-1**, **pDPP4T-2** and **pDPP4T-3**. This agrees with the AFM images of **pDPP4T-1**, **pDPP4T-2** and **pDPP4T-3**.

(42) Zhang, X. R.; Bronstein, H.; Kronemeijer, A. J.; Smith, J.; Kim, Y.; Kline, R. J.; Richter, L. J.; Anthopoulos, T. D.; Sirringhaus, H.; Song, K.; Heeney, M.; Zhang, W. M.; McCulloch, I.; DeLongchamp, D. M. *Nat. Commun.* **2013**, *4*, 2238.

(43) McCulloch, I.; Heeney, M.; Bailey, C.; Genevicius, K.; MacDonald, I.; Shkunov, M.; Sparrowe, D.; Tierney, S.; Wagner, R.; Zhang, W.; Chabinyc, M. L.; Kline, R. J.; McGehee, M. D.; Toney, M. F. *Nat. Mater.* **2006**, *5*, 328.

(44) (a) Liu, F.; Gu, Y.; Wang, C.; Zhao, W.; Chen, D.; Briseno, A. L.; Russell, T. P. *Adv. Mater.* **2012**, *24*, 3947. (b) Li, W.; Yang, L.; Tumbleston, J. R.; Yan, L.; Ade, H.; You, W. *Adv. Mater.* **2014**, *26*, 4456. (c) Bartelt, J. A.; Douglas, J. D.; Mateker, W. R.; Labban, A. E.; Tassone, C. J.; Toney, M. F.; Fréchet, J. M. J.; Beaujuge, P. M.; McGehee, M. D. *Adv. Energy Mater.* **2014**, *4*, 1301733. (d) Liu, C.; Wang, K.; Hu, X.; Yang, Y.; Hsu, C.-H.; Zhang, W.; Xiao, S.; Gong, X.; Cao, Y. *ACS Appl. Mater. Interfaces* **2013**, *5*, 12163.

(45) (a) Guo, X.; Zhang, M. J.; Tan, J. H.; Zhang, S. Q.; Huo, L. J.; Hu, W. P.; Li, Y. F.; Hou, J. H. *Adv. Mater.* **2012**, *24*, 6536. (b) Heeger, A. J. *Adv. Mater.* **2014**, *26*, 10. (c) Huang, Y.; Kramer, E. J.; Heeger, A. J.; Bazan, G. C. *Chem. Rev.* **2014**, *114*, 7006. (d) Yiu, A. T.; Beaujuge, P. M.; Lee, O. P.; Woo, C. H.; Toney, M. F.; Fréchet, J. M. J. *J. Am. Chem. Soc.* **2012**, *134*, 2180. (e) Zhou, J. Y.; Wan, X. J.; Liu, Y. S.; Zuo, Y.; Li, Z.; He, G. R.; Long, G. K.; Ni, W.; Li, C. X.; Su, X. C.; Chen, Y. S. *J. Am. Chem. Soc.* **2012**, *134*, 16345. (f) Lin, Y.; Lim, J. A.; Wei, Q.; Mannsfeld, S. C. B.; Briseno, A. L.; Watkins, J. J. *Chem. Mater.* **2012**, *24*, 622.

(46) (a) Li, W. W.; Hendriks, K. H.; Furlan, A.; Roelofs, W. S. C.; Wienk, M. M.; Janssen, R. A. J. *J. Am. Chem. Soc.* **2013**, *135*, 18942. (b) Li, W. W.; Hendriks, K. H.; Furlan, A.; Roelofs, W. S. C.; Meskers, S. C. J.; Wienk, M. M.; Janssen, R. A. J. *Adv. Mater.* **2014**, *26*, 1565. (c) Li, W. W.; Furlan, A.; Roelofs, W. S. C.; Hendriks, K. H.; van Pruissen, G. W. P.; Wienk, M. M.; Janssen, R. A. J. *Chem. Commun.* **2014**, *50*, 679.

(47) (a) Guo, J.; Liang, Y.; Szarko, J.; Lee, B.; Son, H. J.; Rolczynski, B. S.; Yu, L.; Chen, L. X. *J. Phys. Chem. B* **2010**, *114*, 742. (b) Verploegen, E.; Mondal, R.; Bettinger, C. J.; Sok, S.; Toney, M. F.; Bao, Z. N. *Adv. Funct. Mater.* **2010**, *20*, 3519.

DOI: 10.1021/jacs.5b09737
J. Am. Chem. Soc. 2016, 138, 173−185